To the Graduate Council:

I am submitting herewith a thesis written by James Barney Holt entitled "Three-Dimensional Flows in the Vicinity of the Hair Cells of the Cochlea." I have examined the final copy of this thesis for form and content and recommend that it be accepted in partial fulfillment of the requirements for the degree of Master of Science, with a major in Engineering Science.

Joseph A. M. Boulet, Major Professor

We have read this thesis and recommend its acceptance:

Accepted for the Council:

Vice Provost and
Dean of the Graduate School

STATEMENT OF PERMISSION TO USE

In presenting this thesis in partial fulfillment of the requirements for a Master's degree at The University of Tennessee, Knoxville, I agree that the Library shall make it available to borrowers under rules of the Library. Brief quotations from this thesis are allowable without special permission, provided that accurate acknowledgment of the source is made.

Permission for extensive quotation from or reproduction of this thesis may be granted by my major professor, or in his absence, by the Head of Interlibrary Services when, in the opinion of either, the proposed use of the material is for scholarly purposes. Any copying or use of the material in this thesis for financial gain shall not be allowed without my written permission.

Signature James Barney Holt

Date May 13, 1986

THREE-DIMENSIONAL FLOWS IN THE VICINITY OF THE HAIR CELLS OF THE COCHLEA

A Thesis

Presented for the

Master of Science

Degree

The University of Tennessee, Knoxville

James Barney Holt

June 1986

ACKNOWLEDGMENTS

I am indebted to my advisor, Dr. Joseph A. M. Boulet, for his constant guidance and encouragement in support of this work.

For their contributions to this work, I am grateful to both Dr. Thomas G. Carley and Dr. Osama Soliman.

Recognition is given to The University of Tennessee's Department of Engineering Science and Mechanics for their financial support.

Finally, to my family I express my gratitude and love: especially to my mother Colene and my father Gene and to my fiancée Kimberly Jones.

ABSTRACT

The cochlea is the spiral-shaped part of the inner ear in which mechanical waves are transformed to neural output. It is the hair cells residing in the narrow gap between the tectorial membrane and organ of Corti that are considered to be the primary transducers of the hearing mechanism. For the first time, three-dimensional flow fields are obtained in the vicinity of the hair cells. The resulting flow fields are then incorporated into an existing numerical simulation.

Three-dimensional analysis of the gap flow induced by displacement of the tectorial membrane and organ of Corti yields results that differ qualitatively, but not quantitatively, from those of a two-dimensional analysis.

In addition to the flow induced by membrane displacements, the net flow through the gap, which is driven by pressures in scala vestibuli and the inner sulcus, is analyzed. Three-dimensional analysis indicates that the model may admit three modes of propagation.

TABLE OF CONTENTS

SECTION		PAGE
1.	INTRODUCTION	1
2.	VARIATIONAL EQUATIONS	5
3.	TIME-AVERAGED LAGRANGIAN	8
4.	GAP FLOWS	11
	4.1. General Description	11
	4.2. Net Flow	15
	4.3. Flow Induced by Relative Motion of the Gap Boundaries	19
	4.3.1. Horizontal Displacement	19
	4.3.2. Vertical Displacement	21
	4.3.3. Rotational Displacement	27
	4.4. Gap Springs	29
5.	SYSTEM ENERGY	42
	5.1. Partition Energy	42
	5.2. Gap Flow Inertia	47
	5.3. Duct Flow Inertia	47
6.	DISPERSION RELATION	49
7.	DATA	52
8.	RESULTS	55
	8.1. Stiffness Terms	55
	8.2. Wavenumbers	60
9.	CONCLUSIONS	64
LIST OF REFERENCES		66
VITA		68

LIST OF FIGURES

FIGURE		PAGE
1.1.	Cross Section of the Mammalian Cochlear Duct	2
1.2.	Cross Section of the Partition, Helle's Model G2 [Boulet (1984)]	4
4.1.	Gap Flow Coordinates	13
4.2.	Fluid Flow Patterns Due to Pressures	17
4.3.	System Displacements	20
4.4.	Fluid Flow Patterns Due to Vertical Displacement	25
4.5.	Fluid Flow in the yz Plane Due to Vertical Displacement .	26
4.6.	Fluid Flow Patterns Due to Rotation	30
4.7.	Fluid Flow in the yz Plane Due to Rotation	31
4.8.	Resistive Fluid Forces on the Organ of Corti and Tectorial Membrane Beams	32
4.9.	Spring-Mass-Damper System with Harmonic Excitation	36
8.1.	Imaginary vs. Real, Complex Vertical Spring Stiffness, 70 Hz	56
8.2.	Imaginary vs. Real, Complex Rotational Spring Stiffness, 70 Hz	57
8.3.	Vertical Spring Stiffness vs. Distance from Stapes, 70 Hz	58
8.4.	Rotational Spring Stiffness vs. Distance from Stapes, 70 Hz	59
8.5.	Imaginary vs. Real, Complex Wavenumber, Mode 1, 70 Hz., Two-Dimensional and Three-Dimensional Models	61
8.6.	Imaginary vs. Real, Complex Wavenumber, Mode 2, 70 Hz., Two-Dimensional and Three-Dimensional Models	62

1. INTRODUCTION

The work described herein incorporates a three-dimensional flow analysis into a numerical simulation of the mammalian cochlea (inner ear) developed by Boulet (1984). The flow being analyzed is in the narrow gap between the tectorial and basilar membranes (see Figure 1.1). The cochlear model described by Boulet does not include a three-dimensional flow analysis in the gap and will be referred to as the two-dimensional model. The improved cochlear model will be called the three-dimensional model. Those portions of the simulation not related to the gap flow were derived by Boulet and will be quoted from his work as needed.

It is hoped that the three-dimensional model will help gain a better understanding of the mammalian hearing mechanism. The hair cells residing in the gap are considered the primary transducers of mechanical input (stapes vibration) to neural output. At present, the stimulation process of the hair cells is unknown. New insight into this mechanism may be gained from studying the flow fields in the vicinity of the hair cells. The present work describes derivation of three-dimensional flow fields in this region and their incorporation into the existing numerical simulation. It is also hoped that these new flow fields will improve agreement between the numerical simulation and the physical results of previous experiments.

The physical model from which the numerical simulation is formulated is Helle's model G2 [Helle (1974)]. A cross section of the

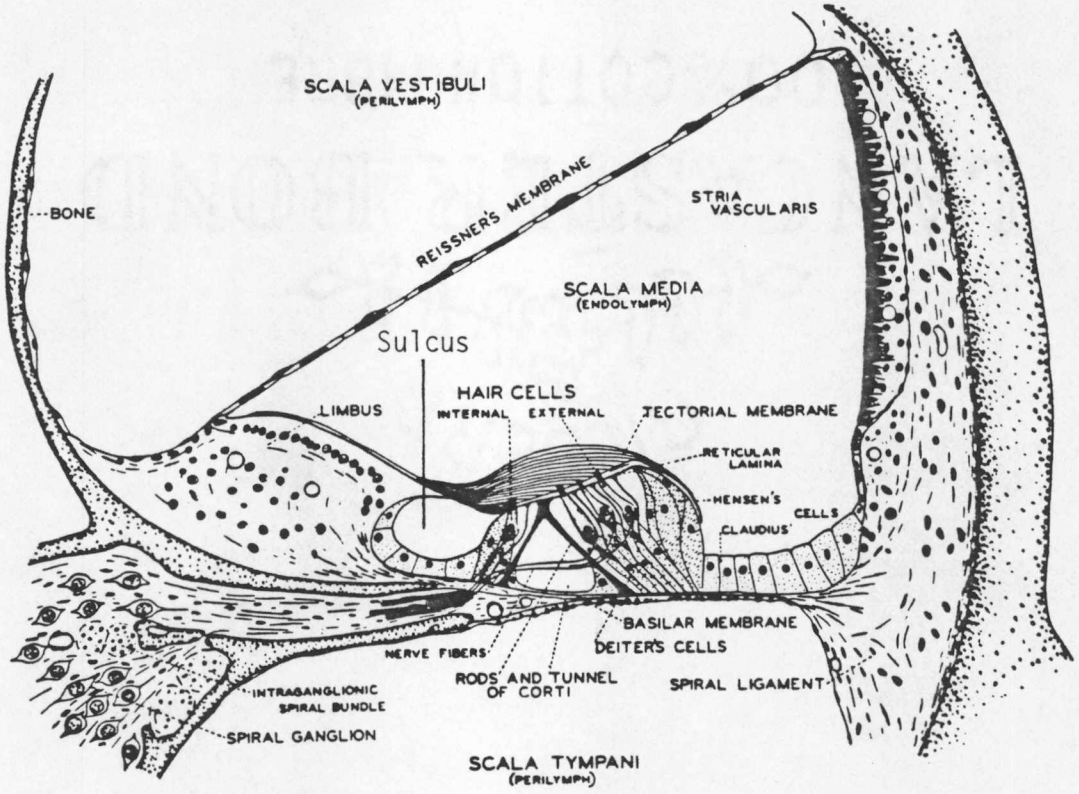


Figure 1.1. Cross Section of the Mammalian Cochlear Duct. [Davis (1953).]

model is shown in Figure 1.2. The model's length normal to the figure is more than ten times its greatest dimension in the plane of the figure. The fluid pressures in the three ducts, scala vestibuli (SV), scala tympani (ST), and the inner sulcus, will hereafter be referred to as p_1, p_2, and p_3, respectively. The complicated structure separating SV and ST will be referred to as the cochlear partition. The spiral limbus, the aluminum plate, and the plexiglas will be considered rigid, while linear, elastic behavior will be assumed for the rubber structures. The three slender regions of width b_1, b_2, and b_3 in Figure 1.2 will be referred to as "membranes." The two thicker regions of width c in Figure 1.2 will be referred to as "blocks," even though their greatest dimension is normal to the cross section of the partition. Hence, the elastic portion of the partition in Figure 1.2 consists of the basilar membrane (BM), sulcus floor, tectorial membrane (TM), organ of Corti (OC) block, and the TM block [Boulet (1984)]. The properties considered in the simulation include geometry, elastic constants, and viscosity and density of the fluid in the ducts.

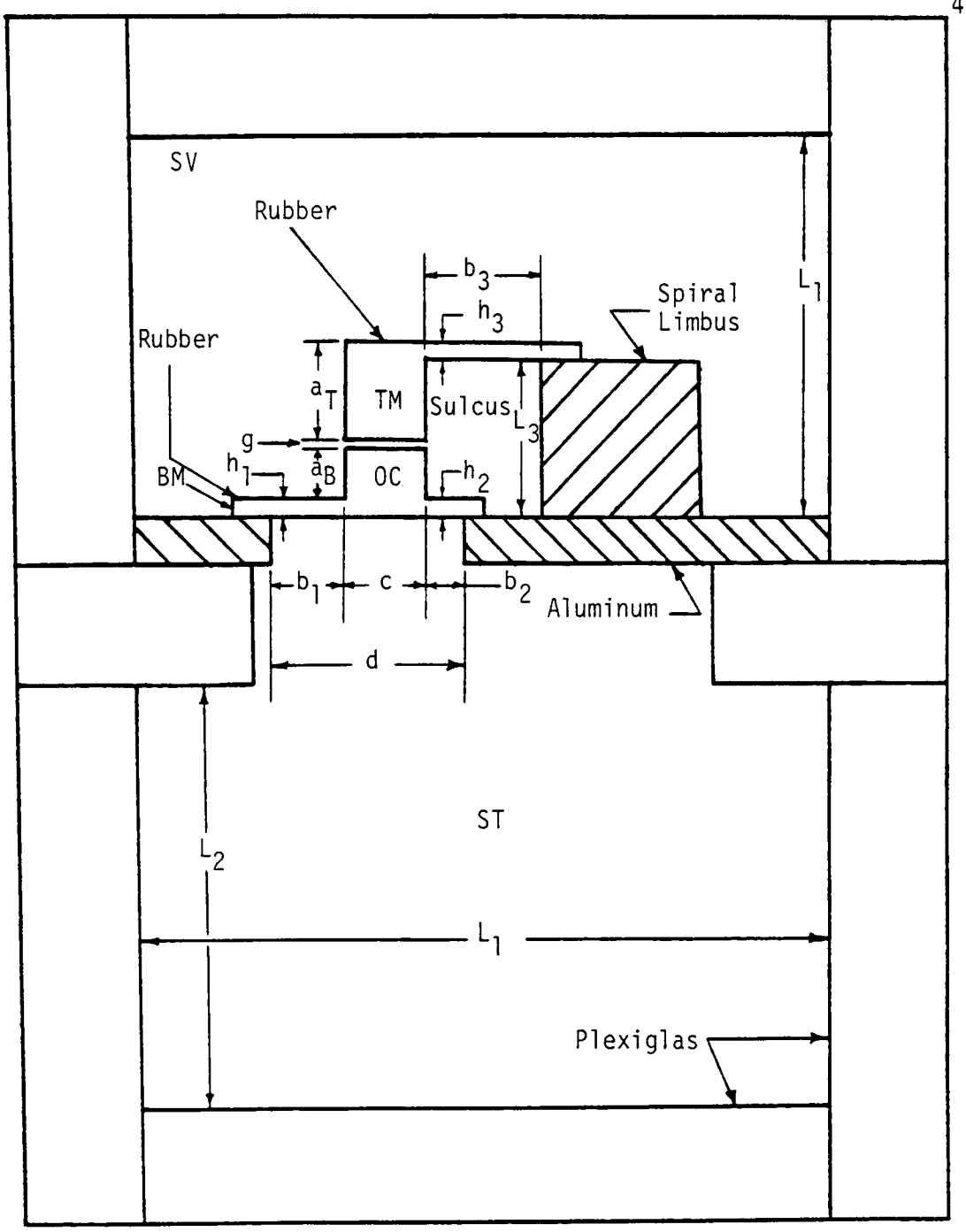


Figure 1.2. Cross Section of the Partition, Helle's Model G2 [Boulet (1984)]. Numerical Values of all Dimensions Are Given in Section 7.

2. VARIATIONAL EQUATIONS

The physical dimensions of the cochlear duct change significantly along the length of the cochlea. Therefore, propagating waves resulting from stapes vibration disperse. Both the amplitudes and wavenumbers of these waves depend on their distance down the cochlear duct. Nevertheless, we assume that at any position, x, and at any time, t, the phase, θ, can be found by integrating the wavenumber, λ, with respect to x. Thus, following Steele (1974), we assume the phase integral form for x-direction propagation, which is

$$p(x,t) = P(x)\mathrm{Re}(e^{i\theta}) \ , \tag{2.1}$$

$$\theta = \omega t - \int \lambda(x)dx \ , \tag{2.2}$$

where $p(x,t)$, $P(x)$, and ω are any propagating quantity, its amplitude function, and the excitation frequency, respectively. The phase integral form is appropriate whenever the wavenumber and amplitude function are "slowly varying" in the sense that they change little over one wavelength. For the most part, traveling waves in the cochlea satisfy this condition. This is so because the geometry of the cochlear duct changes gradually from one end to the other.

The assumption of a slowly varying solution, usually referred to as the WKB assumption, has been used in a wide variety of circumstances, many of which are discussed by Steele (1976). In particular, Whitham (1974) describes the use of the WKB assumption together with

the Euler-Lagrange variational equations. For two independent variables, x and t, the Euler-Lagrange variational equations are

$$\frac{\partial L}{\partial P} - \frac{\partial}{\partial t}\left(\frac{\partial L}{\partial \dot{P}}\right) - \frac{\partial}{\partial x}\left(\frac{\partial L}{\partial P'}\right) = 0 \ , \tag{2.3a}$$

$$\frac{\partial L}{\partial \theta} - \frac{\partial}{\partial t}\left(\frac{\partial L}{\partial \dot{\theta}}\right) - \frac{\partial}{\partial x}\left(\frac{\partial L}{\partial \theta'}\right) = 0 \ , \tag{2.3b}$$

where L is the Lagrangian of the system and the superior dot and the prime indicate differentiation with respect to time and x, respectively. Using the WKB assumption, we see that the third term of Eq. (2.3a) should be ignored. For steady-state response, the second terms of Eqs. (2.3) are also neglected. Therefore, Eqs. (2.3) become

$$\frac{\partial L}{\partial P} = 0 \ , \tag{2.4a}$$

$$\frac{\partial L}{\partial \theta} - \frac{\partial}{\partial x}\left(\frac{\partial L}{\partial \theta'}\right) = 0 \ . \tag{2.4b}$$

Whitham has shown that when the WKB assumption applies, Eqs. (2.4) apply to the average value of the Lagrangian over one cycle. Hence, we discard L in favor of the phase-averaged Lagrangian, which is

$$\mathcal{L} = \frac{1}{2\pi}\int_0^{2\pi} L \, d\theta \ . \tag{2.5}$$

Applying Eq. (2.5) to Eqs. (2.4), we get

$$\frac{\partial L}{\partial P} = 0 \ , \tag{2.6a}$$

$$\frac{\partial}{\partial x}\left(\frac{\partial L}{\partial \theta'}\right) = 0 \ . \tag{2.6b}$$

Equation (2.6a) will be used in Section 3 to obtain the dispersion relation and is referred to as the "eikonal" equation. Equation (2.6b) is the transport equation and gives the dependence of the amplitude on x.

3. TIME-AVERAGED LAGRANGIAN

The time-averaged Lagrangian for the system is defined by

$$L = T - U \quad , \tag{3.1}$$

where T is the total time-averaged kinetic energy and U is the total time-averaged potential energy. The total potential energy is the potential energy of the partition (see Section 5). Therefore, the total time-averaged potential energy is

$$U = (1/4)\{P\}^T[C]\{P\} \quad , \tag{3.2}$$

where [C] is the compliance matrix (see Section 5), and the elements of {P} are amplitudes of the previously mentioned pressures p_1, p_2, and p_3. The time-averaged kinetic energy of the duct fluid and the gap fluid combine to yield the total time-averaged kinetic energy which can be written as

$$T = T_D + T_G \quad , \tag{3.3a}$$

where

$$T_D = (1/4)\{P\}^T[G]\{P\} \quad , \tag{3.3b}$$

$$T_G = (1/4)\{P\}^T[G_G]\{P\} \quad , \tag{3.3c}$$

and [G] and $[G_G]$ are the duct and gap flow inertia matrices, respectively. Thus, from Eqs. (3.1), (3.2), and (3.3), we find

$$L = (1/4)\{P\}^T[D]\{P\} , \tag{3.4}$$

where the dynamic matrix, [D], is defined as

$$[D] = [G] + [G_G] - [C] . \tag{3.5}$$

Following Boulet (1984), we write Eq. (3.4) with the pressure vector in magnitude/unit vector form as

$$L = (1/4)P^2(x)\{\alpha\}^T[D]\{\alpha\} , \tag{3.6}$$

where

$$P(x) = (P_1^2 + P_2^2 + P_3^2)^{1/2} , \tag{3.7a}$$

$$\|\alpha\| = 1 , \tag{3.7b}$$

$$\{P\} = P(x)\{\alpha\} . \tag{3.7c}$$

For a nontrivial solution of the eikonal equation, Eq. (2.6a), and Eq. (3.6),

$$\{\alpha\}^T[D]\{\alpha\} = 0 , \tag{3.8a}$$

$$[D]\{\alpha\} = 0 , \tag{3.8b}$$

$$F(\xi,\omega) = 0 , \tag{3.8c}$$

where

$$F(\xi,\omega) = |D| , \tag{3.8d}$$

$$\xi = \lambda L_2 . \tag{3.8e}$$

The dispersion relation is Eq. (3.8c) and the roots of the dispersion function $F(\xi,\omega)$ are dimensionless wavenumbers of the system response.

4. GAP FLOWS

4.1. General Description

The flow field in the gap between the tectorial membrane block and the organ of Corti block is induced by the pressures in the sulcus and scala vestibuli, and also by the motion of the blocks. By superposition of these two parts, we can obtain the complete flow field in the gap.

The net flow between the sulcus and scala vestibuli is the part of the flow induced by the duct pressures. The kinetic energy of this flow is included in the kinetic energy of the system. In the other part of the flow, the pressures in the two ducts, as well as the net transfer of fluid through the gap, are zero. Instead, motion of the blocks occurs, and the fluid in the gap resists the motion. This resistance takes the form of stresses exerted on the blocks by the gap fluid during the block motion. These stresses can be integrated over the surfaces of the blocks to obtain load-deflection relationships for hypothetical "fluid springs" in the gap. From these relationships, we can determine the "spring stiffnesses" associated with the fluid resistance. Then the "potential energy" of these "fluid springs" is included in the potential energy of the partition [Boulet (1984)]. (The term "fluid springs" is associated with the fluid forces resisting block motion. These forces arise because of the fluid's kinetic energy and viscous dissipation, and are not

associated with compressibility of the fluid.) Derivations of the net flow kinetic energy, and the spring stiffnesses, are shown below.

As mentioned previously, the solutions discussed below are three-dimensional. They include three orthogonal velocity components and they satisfy the local continuity equation everywhere. In contrast, the two-dimensional solutions of Boulet (1984) account for flow in only one direction and satisfy only a global (control-volume) form of the continuity equation.

The coordinate system defined in Figure 4.1 is used throughout the three-dimensional gap fluid analysis. For constant fluid properties and small displacements, the desired equations of motion are the linearized Navier-Stokes equations. These equations can be represented by a single vector equation written as

$$\rho \frac{\partial \dot{\overline{V}}}{\partial t} = - \overline{\nabla} p + \mu \nabla^2 \dot{\overline{V}} \ , \tag{4.1}$$

where

$$\dot{\overline{V}} = \dot{u}\hat{i} + \dot{v}\hat{j} + \dot{w}\hat{k} \ , \tag{4.2a}$$

$$\dot{u} = f(x,y,z,t) \ , \tag{4.2b}$$

$$\dot{v} = g(x,y,z,t) \ , \tag{4.2c}$$

$$\dot{w} = h(x,y,z,t) \ , \tag{4.2d}$$

$$p = q(x,y,z,t) \ . \tag{4.2e}$$

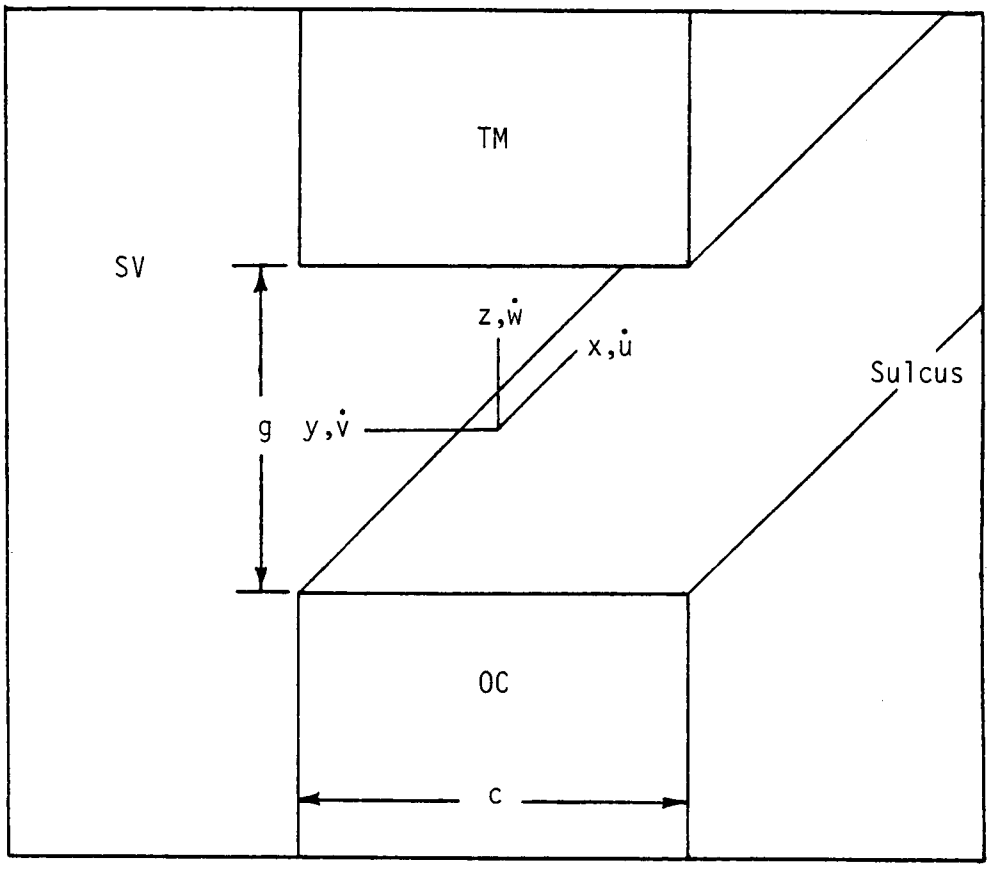


Figure 4.1. Gap Flow Coordinates. These Coordinates Are Used in All Three-Dimensional Gap Flow Analysis.

For solutions propagating in the x-direction Eqs. (4.2) can be written as

$$\dot{u} = \mathrm{Re}[f(y,z)e^{i\theta}] \ , \tag{4.3a}$$

$$\dot{v} = \mathrm{Re}[g(y,z)e^{i\theta}] \ , \tag{4.3b}$$

$$\dot{w} = \mathrm{Re}[h(y,z)e^{i\theta}] \ , \tag{4.3c}$$

$$p = \mathrm{Re}[q(y,z)e^{i\theta}] \ , \tag{4.3d}$$

where the phase, θ, has a period of $2\pi/\lambda$. A fourth equation relating the components of the velocity is the continuity equation. The general form of the equation of continuity for fluids is

$$\frac{\partial \rho}{\partial t} + \nabla \cdot \rho\dot{\overline{V}} = 0 \ . \tag{4.4}$$

For constant density, Eq. (4.4) reduces to

$$\nabla \cdot \dot{\overline{V}} = 0 \ . \tag{4.5}$$

Assuming the phase integral form, we can rewrite Eqs. (4.1) and (4.5) as

$$\frac{\partial^2 \dot{\overline{V}}}{\partial y^2} + \frac{\partial^2 \dot{\overline{V}}}{\partial z^2} - \beta^2 \dot{\overline{V}} = \frac{1}{\mu}\left(\frac{\partial p}{\partial y}\hat{j} + \frac{\partial p}{\partial z}\hat{k}\right) - i\lambda p\hat{i} \ , \tag{4.6a}$$

$$- i\lambda\dot{u} + \frac{\partial \dot{v}}{\partial y} + \frac{\partial \dot{w}}{\partial z} = 0 \ , \tag{4.6b}$$

respectively, where

$$\beta^2 = \lambda^2 + \frac{i\rho\omega}{\mu} \ . \tag{4.6c}$$

4.2. Net Flow

For the net flow through the gap, the no-slip boundary conditions at the upper and lower gap boundaries are

$$\dot{u}\Big|_{z=\pm g/2} = 0 \ , \tag{4.7a}$$

$$\dot{v}\Big|_{z=\pm g/2} = 0 \ , \tag{4.7b}$$

$$\dot{w}\Big|_{z=\pm g/2} = 0 \ . \tag{4.7c}$$

When we assume the pressure has no z dependence, the proper boundary conditions are

$$p\Big|_{y=c/2} = p_1 \ , \tag{4.8a}$$

$$p\Big|_{y=-c/2} = p_3 \ , \tag{4.8b}$$

where p_1 and p_3 are the pressures in scala vestibuli and sulcus, respectively. The solutions of Eqs. (4.6) that satisfy Eqs. (4.7) and (4.8) are

$$\dot{u} = \frac{\lambda \bar{p}}{\rho\omega}\left(\frac{\cosh(\lambda y)}{\cosh \eta} + \frac{\alpha \sinh(\lambda y)}{\sinh \eta}\right)\left(1 - \frac{\cosh(\beta z)}{\cosh \gamma}\right) \ , \tag{4.9a}$$

$$\dot{v} = \frac{i\lambda \bar{p}}{\rho\omega}\left(\frac{\sinh(\lambda y)}{\cosh \eta} + \frac{\alpha \cosh(\lambda y)}{\sinh \eta}\right)\left(1 - \frac{\cosh(\beta z)}{\cosh \gamma}\right) \ , \tag{4.9b}$$

$$\dot{w} = 0 \ , \tag{4.9c}$$

and

$$p = \bar{p}\left[\frac{\cosh(\lambda y)}{\cosh \eta} + \frac{\alpha \sinh(\lambda y)}{\sinh \eta}\right] , \tag{4.9d}$$

where

$$\eta = \frac{\lambda c}{2} , \tag{4.9e}$$

$$\gamma = \frac{\beta g}{2} , \tag{4.9f}$$

$$\bar{p} = \frac{p_1 + p_3}{2} , \tag{4.9g}$$

$$\alpha = \frac{p_1 - p_3}{p_1 + p_3} . \tag{4.9h}$$

and β is defined by Eq. (4.6c). The solutions for the two-dimensional model [see Boulet (1984)] are

$$\dot{v} = \frac{p_3 - p_1}{c\mu\beta^2}\left[1 - \frac{\cosh(\beta z)}{\cosh \gamma}\right] , \tag{4.10a}$$

and

$$p = \frac{1}{2}(p_1 + p_3) + (p_1 - p_3)\frac{y}{c} . \tag{4.10b}$$

Comparing the solutions of the two models, we find an additional velocity component in the x-direction in the three-dimensional model. This component is apparently just as significant as the y-component. The new x-component and the additional term in the y-component add fluid streaming along the duct and across both sides of the gap (see Figure 4.2). As a result of the $\dot{v}$ velocity terms, fluid shoots into

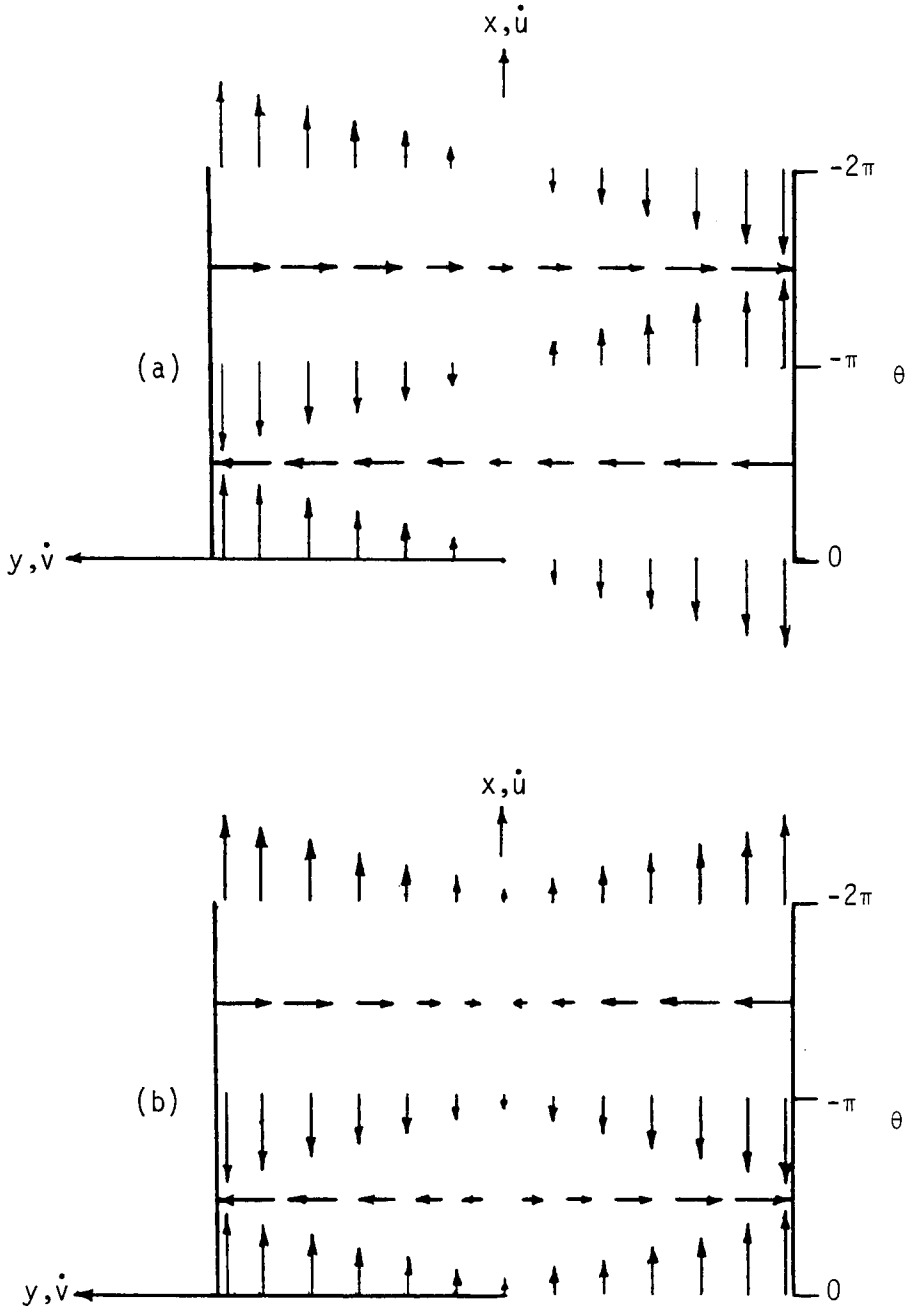


Figure 4.2. Fluid Flow Patterns Due to Pressures. Length of θ is $2\pi/\lambda$, the Period of the Phase, and y is from c/2 to -c/2. Patterns Are Due to (a) Pressure Difference, and (b) Pressure Addition ($p_1 + p_3$).

and out from the center of the gap. This fluid must be "fed" by the $\dot{u}$ velocity terms which move fluid along the duct. The three-dimensional solutions also exhibit a dependence on wavenumber. However, as $\lambda \to 0$ the three-dimensional solutions, Eqs. (4.9), reduce to the two-dimensional solutions, Eqs. (4.10), found by Boulet. Thus, for very small wavenumbers $\dot{v}$ dominates the flow field.

The time-averaged kinetic energy per unit length in the x-direction for the three-dimensional net gap flow is

$$\mathcal{T}_G = \frac{1}{2\pi} \int_0^{2\pi} T d\theta \ , \tag{4.11a}$$

where

$$T = \frac{1}{2} \rho \int_{-c/2}^{c/2} \int_{-g/2}^{g/2} (\dot{u}^2 + \dot{v}^2 + \dot{w}^2) dz dy \ . \tag{4.11b}$$

From Eqs. (4.9) and (4.11), we obtain

$$\mathcal{T}_G = (1/4)[S_1(p_1 + p_3)^2 + S_2(p_1 - p_3)^2] \ , \tag{4.12a}$$

where

$$S_1 = \frac{4\eta \tanh \eta}{\beta \rho \omega^2 c} [3(\gamma - \tanh \gamma) - \gamma \tanh^2 \gamma] \ , \tag{4.12b}$$

$$S_2 = \frac{S_1}{\tanh^2 \eta} \ . \tag{4.12c}$$

4.3. Flow Induced by Relative Motion of the Gap Boundaries

Displacements of the partition are shown in Figure 4.3. The η_1, η_2, and η_3 are average displacements of the basilar membrane, sulcus floor, and tectorial membrane, respectively, due to uniform pressure differences alone, and will be used later to compute the potential energy of the partition. Motion of the gap boundaries can be described using the other four displacements shown in Figure 4.3. Displacements of the block-like portions of the membranes can be resolved into three parts, namely, horizontal translation, vertical translation, and rotation. The flow field induced by each of these is analyzed separately, below. Superposition of the three flows gives the entire induced flow field.

4.3.1. Horizontal Displacement

For the horizontal displacement, the appropriate boundary conditions are

$$\dot{u}\Big|_{z=\pm g/2} = 0 \ , \tag{4.13a}$$

$$\dot{v}\Big|_{z=g/2} = -a_T\dot{X}_T \ , \tag{4.13b}$$

$$\dot{v}\Big|_{z=-g/2} = -a_B\dot{X}_B \ , \tag{4.13c}$$

$$\dot{w}\Big|_{z=\pm g/2} = 0 \ , \tag{4.13d}$$

$$p\Big|_{y=\pm c/2} = 0 \ . \tag{4.13e}$$

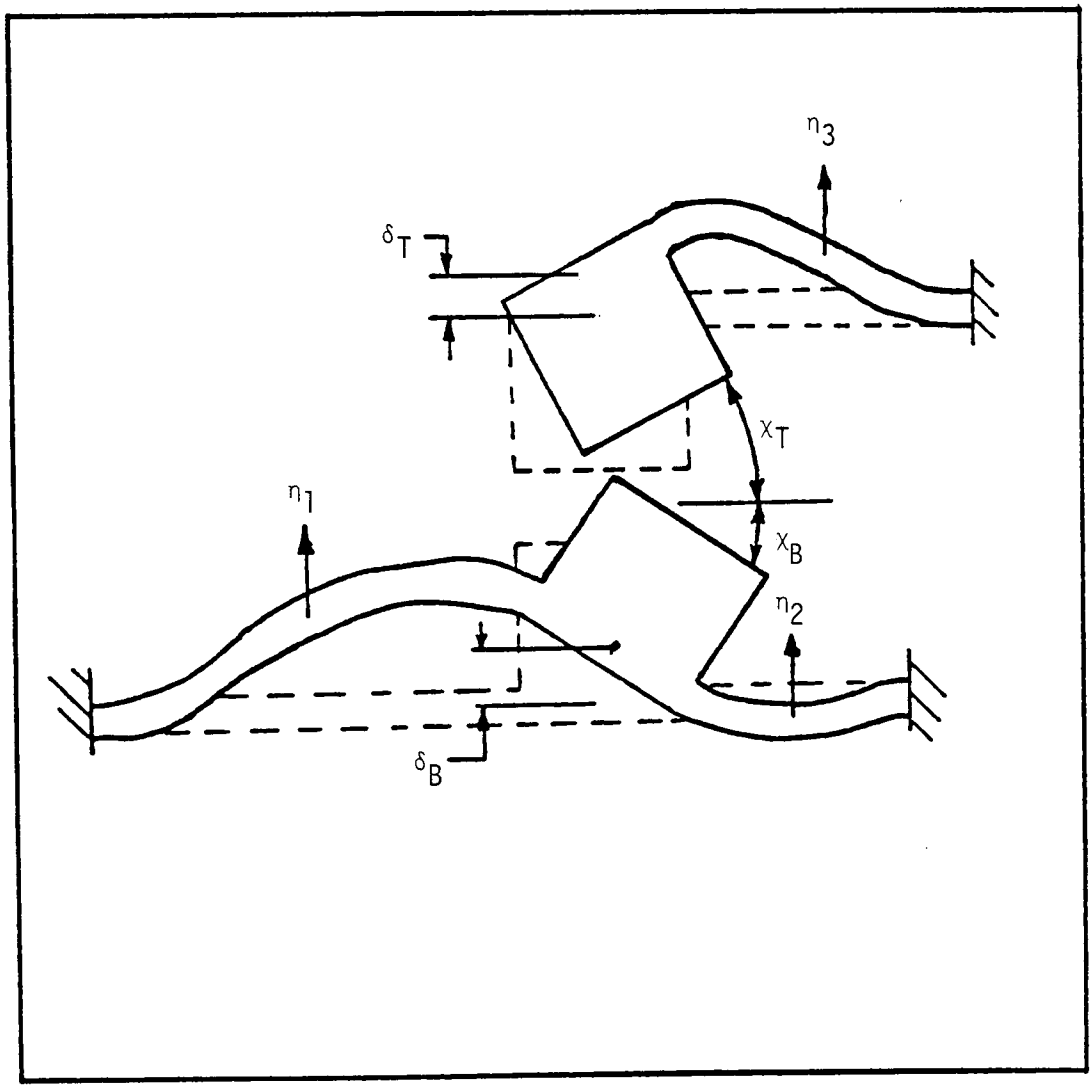


Figure 4.3. System Displacements. Original Partition Energies Are Determined with These [Boulet (1984)].

The solutions of Eqs. (4.6) that satisfy Eqs. (4.13) are

$$\dot{u} = 0 \ , \tag{4.14a}$$

$$\dot{v} = \frac{-\dot{\chi}_S \cosh(\beta z)}{2 \cosh \gamma} + \frac{\dot{\chi}_D \sinh(\beta z)}{2 \sinh \gamma} \ , \tag{4.14b}$$

$$\dot{w} = 0 \ , \tag{4.14c}$$

$$p = 0 \ , \tag{4.14d}$$

where

$$\dot{\chi}_S = a_B \dot{\chi}_B + a_T \dot{\chi}_T \ , \tag{4.14e}$$

$$\dot{\chi}_D = a_B \dot{\chi}_B - a_T \dot{\chi}_T \ . \tag{4.14f}$$

These solutions are identical to the two-dimensional solutions obtained by Boulet.

4.3.2. Vertical Displacement

For the vertical displacement, the boundary conditions are

$$\dot{u}\Big|_{z=\pm g/2} = 0 \ , \tag{4.15a}$$

$$\dot{v}\Big|_{z=\pm g/2} = 0 \ , \tag{4.15b}$$

$$\dot{w}\Big|_{z=g/2} = \dot{\delta}_T \ , \tag{4.15c}$$

$$\dot{w}\Big|_{z=-g/2} = \dot{\delta}_B \ , \tag{4.15d}$$

and

$$p\Big|_{y=\pm c/2} = 0 \ . \tag{4.15e}$$

The desired solutions of Eqs. (4.6) that satisfy Eqs. (4.15) require more effort than the two previous parts of the flow field. To satisfy Eqs. (4.15c) and (4.15d), the y dependence must vanish at $z=\pm g/2$. This condition is satisfied by using a nonconstant Fourier series for rectangular pulses to represent the y dependence in the flow field. The resulting solutions of Eqs. (4.6) are

$$\dot{u} = \frac{2i\lambda}{c} \sum_{j=0}^{\infty} \frac{\beta_j G_j(y)}{m_j \alpha_j} \left[\dot{\delta}_{VD} A_j(z) + \dot{\delta}_{VS} B_j(z) \right] , \tag{4.16a}$$

$$\dot{v} = \frac{2}{c} \sum_{j=0}^{\infty} \frac{\beta_j H_j(y)}{m_j} \left[\dot{\delta}_{VS} B_j(z) + \dot{\delta}_{VD} A_j(z) \right] , \tag{4.16b}$$

$$\dot{w} = \frac{2}{c} \sum_{j=0}^{\infty} \frac{G_j(y)}{\alpha_j} \left[\dot{\delta}_{VS} C_j(z) + \dot{\delta}_{VD} D_j(z) \right] , \tag{4.16c}$$

and

$$p = \frac{-2\beta^2 \mu}{c} \sum_{j=0}^{\infty} \frac{\beta_j G_j(y) \cosh \gamma_j}{\alpha_j m_j} \left[\dot{\delta}_{VD} E_j(z) + \dot{\delta}_{VS} F_j(z) \right] , \tag{4.16d}$$

where

$$A_j(z) = \frac{\cosh \eta_j \cosh(\beta_j z) - \cosh \gamma_j \cosh(m_j z)}{\beta_j \tanh \eta_j - m_j \tanh \gamma_j} , \tag{4.16e}$$

$$B_j(z) = \frac{\sinh \eta_j \sinh(\beta_j z) - \sinh \gamma_j \sinh(m_j z)}{\beta_j \tanh \gamma_j - m_j \tanh \eta_j} , \tag{4.16f}$$

$$C_j(z) = \frac{\beta_j \sinh \gamma_j \cosh(m_j z) - m_j \sinh \eta_j \cosh(\beta_j z)}{\beta_j \tanh \gamma_j - m_j \tanh \eta_j} , \qquad (4.16g)$$

$$D_j(z) = \frac{\beta_j \cosh \gamma_j \sinh(m_j z) - m_j \cosh \eta_j \sinh(\beta_j z)}{\beta_j \tanh \eta_j - m_j \tanh \gamma_j} , \qquad (4.16h)$$

$$E_j(z) = \frac{\cosh(m_j z)}{\beta_j \tanh \eta_j - m_j \tanh \gamma_j} , \qquad (4.16i)$$

$$F_j(z) = \frac{\tanh \gamma_j \sinh(m_j z)}{\beta_j \tanh \gamma_j - m_j \tanh \eta_j} , \qquad (4.16j)$$

$$G_j(y) = \frac{(-1)^j \cos(\alpha_j y)}{\cosh \gamma_j \cosh \eta_j} , \qquad (4.16k)$$

$$H_j(y) = \frac{(-1)^j \sin(\alpha_j y)}{\cosh \gamma_j \cosh \eta_j} , \qquad (4.16l)$$

$$\gamma_j = \frac{\beta_j g}{2} , \qquad (4.16m)$$

$$\eta_j = \frac{m_j g}{2} , \qquad (4.16n)$$

$$\beta_j = (m_j^2 + \beta^2)^{1/2} , \qquad (4.16o)$$

$$m_j = (\lambda^2 + \alpha_j^2)^{1/2} , \qquad (4.16p)$$

$$\alpha_j = (2j + 1)\frac{\pi}{c} , \tag{4.16q}$$

$$\dot{\delta}_{VD} = \dot{\delta}_T - \dot{\delta}_B , \tag{4.16r}$$

$$\dot{\delta}_{VS} = \dot{\delta}_T + \dot{\delta}_B , \tag{4.16s}$$

and β is defined by Eq. (4.6c). The two-dimensional solutions derived by Boulet are

$$\dot{v} = -\frac{y}{g}\frac{\gamma}{\gamma - \tanh\gamma}\left(1 - \frac{\cosh(\beta z)}{\cosh\gamma}\right)\dot{\delta}_{VD} , \tag{4.17a}$$

$$p = \frac{3\mu c^2}{2g^3}\left[\left(\frac{2y}{c}\right)^2 - 1\right]\frac{\gamma^3}{3(\gamma - \tanh\gamma)}\dot{\delta}_{VD} , \tag{4.17b}$$

where γ is defined by Eq. (4.9f). The three-dimensional solution has three nonzero velocity components all dependent on wavenumber, while the two-dimensional solution has only one component with no wavenumber dependence. The additional x and z components in the three-dimensional solution add fluid streaming along the duct and vertical movement of fluid in the gap, respectively. The y-component of the velocity moves fluid across the sides of the gap. This movement of fluid by $\dot{v}$ is "fed" by $\dot{u}$ streaming fluid along the duct and $\dot{w}$ moving fluid vertically in the gap. The resulting flow patterns are shown in Figures 4.4 and 4.5.

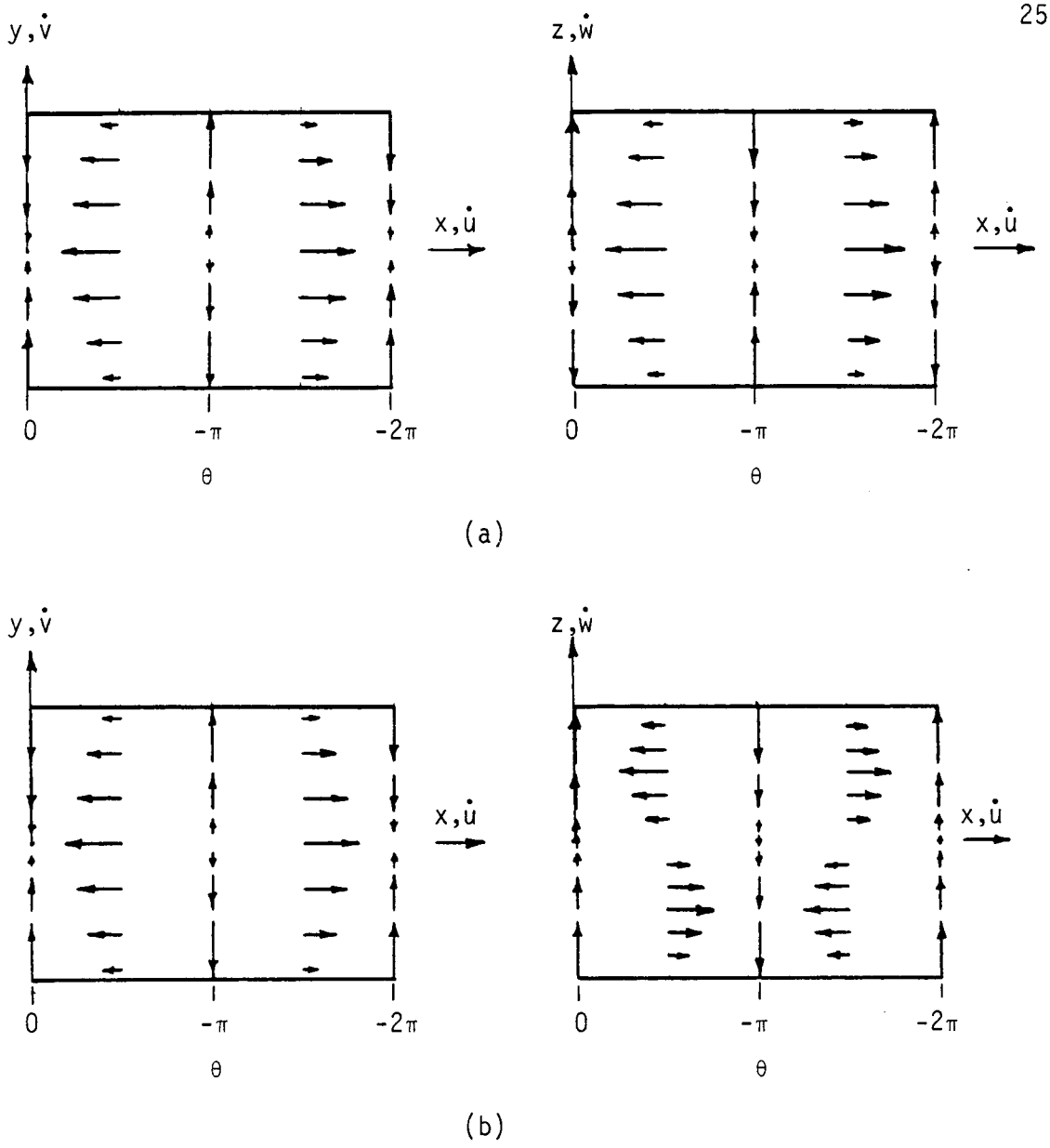


Figure 4.4. Fluid Flow Patterns Due to Vertical Displacement. Length of θ is $2\pi/\lambda$, the Period of the Phase, y is From c/2 to -c/2, and z is From g/2 to -g/2. Patterns Are for (a) Opening or Closing of the Gap, and (b) Rigid Body Displacement of the Gap.

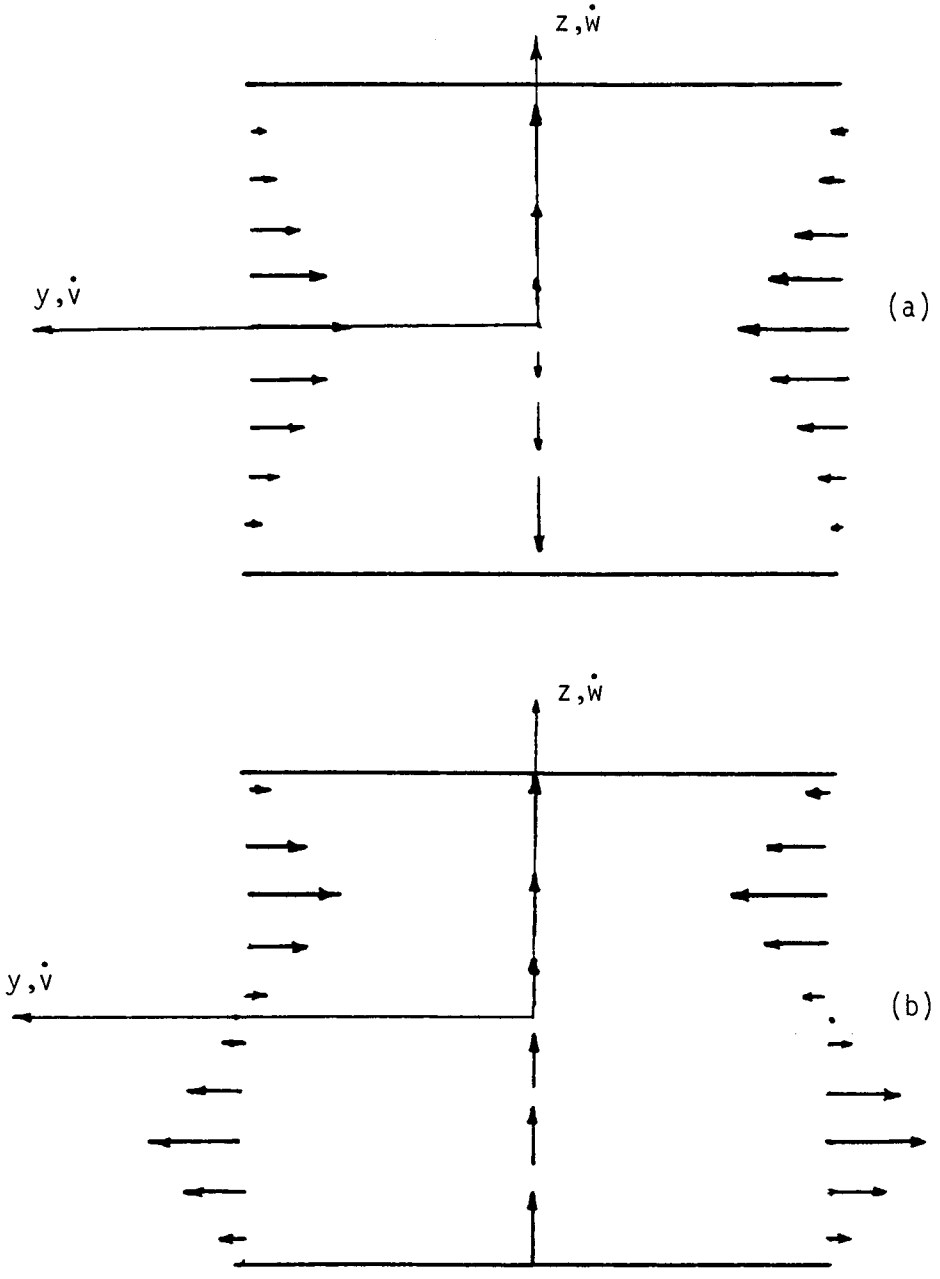


Figure 4.5. Fluid Flow in the yz Plane Due to Vertical Displacement. Bounds on y and z are ±c/2 and ±g/2, Respectively. Patterns Are for (a) Opening or Closing of the Gap, and (b) Rigid Body Displacement of the Gap.

4.3.3. Rotational Displacement

For the rotational displacement, the appropriate boundary conditions are

$$\dot{u}\Big|_{z=\pm g/2} = 0 \ , \tag{4.18a}$$

$$\dot{v}\Big|_{z=\pm g/2} = 0 \ , \tag{4.18b}$$

$$\dot{w}\Big|_{z=g/2} = -y\dot{\chi}_T \ , \tag{4.18c}$$

$$\dot{w}\Big|_{z=-g/2} = y\dot{\chi}_B \ , \tag{4.18d}$$

and

$$p\Big|_{y=\pm c/2} = 0 \ . \tag{4.18e}$$

To satisfy Eqs. (4.18c) and (4.18d) the solutions are expressed as Fourier expansions in y. Therefore, the solutions of Eqs. (4.6) that satisfy Eqs. (4.18) are

$$\dot{u} = -i\lambda \sum_{j=0}^{\infty} \frac{\beta_j R_j(y)}{\alpha_j m_j} \left[\dot{\delta}_{RD} B_j(z) - \dot{\delta}_{RS} A_j(z)\right] \ , \tag{4.19a}$$

$$\dot{v} = \sum_{j=0}^{\infty} \frac{\beta_j P_j(y)}{m_j} \left[\dot{\delta}_{RD} B_j(z) - \dot{\delta}_{RS} A_j(z)\right] \ , \tag{4.19b}$$

$$\dot{w} = \sum_{j=0}^{\infty} \frac{R_j(y)}{\alpha_j} \left[\dot{\delta}_{RS} D_j(z) - \dot{\delta}_{RD} C_j(z)\right] \ , \tag{4.19c}$$

and

$$p = \mu\beta^2 \sum_{j=0}^{\infty} \frac{\beta_j R_j(y)\cosh\gamma_j}{\alpha_j m_j} \left(\dot{\delta}_{RD} F_j(z) - \dot{\delta}_{RS} E_j(z)\right) , \tag{4.19d}$$

where

$$\alpha_j = \frac{2\pi}{c}(j + 1) , \tag{4.19e}$$

$$R_j(y) = \frac{(-1)^{j+1}\sin(\alpha_j y)}{\cosh\gamma_j \cosh\eta_j} , \tag{4.19f}$$

$$P_j(y) = \frac{(-1)^{j+1}\cos(\alpha_j y)}{\cosh\gamma_j \cosh\eta_j} , \tag{4.19g}$$

$$\dot{\delta}_{RD} = \dot{x}_B - \dot{x}_T , \tag{4.19h}$$

$$\dot{\delta}_{RS} = \dot{x}_B + \dot{x}_T , \tag{4.19i}$$

and $A_j(z)$, $B_j(z)$, $C_j(z)$, $D_j(z)$, $E_j(z)$, $F_j(z)$, γ_j, β_j, η_j, and m_j are given by Eqs. (4.16). The corresponding two-dimensional solutions found by Boulet are

$$\dot{v} = \frac{-\dot{\delta}_{RS}}{g} \sum_{j=1}^{\infty} \frac{W_j}{\alpha_j^2} \left(1 - \frac{\cosh(\beta_j z)}{\cosh\gamma_j}\right) \cos(\alpha_j y) , \tag{4.20a}$$

$$p = \frac{\mu\dot{\delta}_{RS}}{g} \sum_{j=1}^{\infty} \frac{\beta_j^2 W_j}{\alpha_j^3} \tag{4.20b}$$

where

$$W_j = (-1)^{j+1} \frac{\gamma_j}{\gamma_j - \tanh \gamma_j} , \tag{4.20c}$$

$$\alpha_j = \frac{2j\pi}{c} . \tag{4.20d}$$

Again the three-dimensional solution has three nonzero velocity components dependent on wavenumber and the two-dimensional solution has one component independent of wavenumber. The x-component of the three-dimensional velocity moves fluid up and down the duct in opposite directions. The flow patterns due to rotational displacement are shown in Figures 4.6 and 4.7.

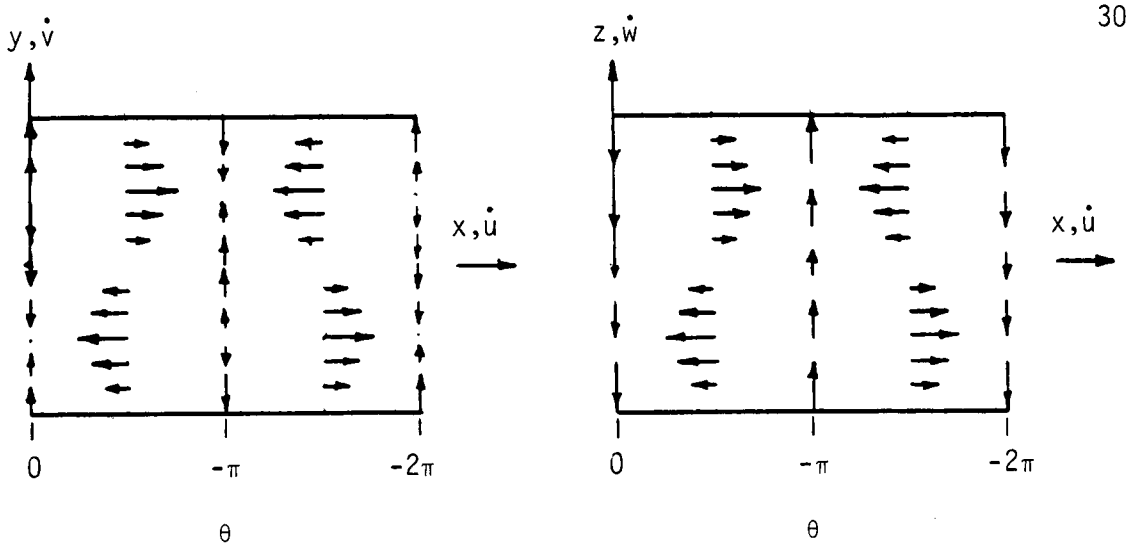
4.4. Gap Springs

The resistive forces of the fluid are shown in Figure 4.8. These forces can be determined from the stresses exerted on the blocks by the gap fluid. The proper expressions are

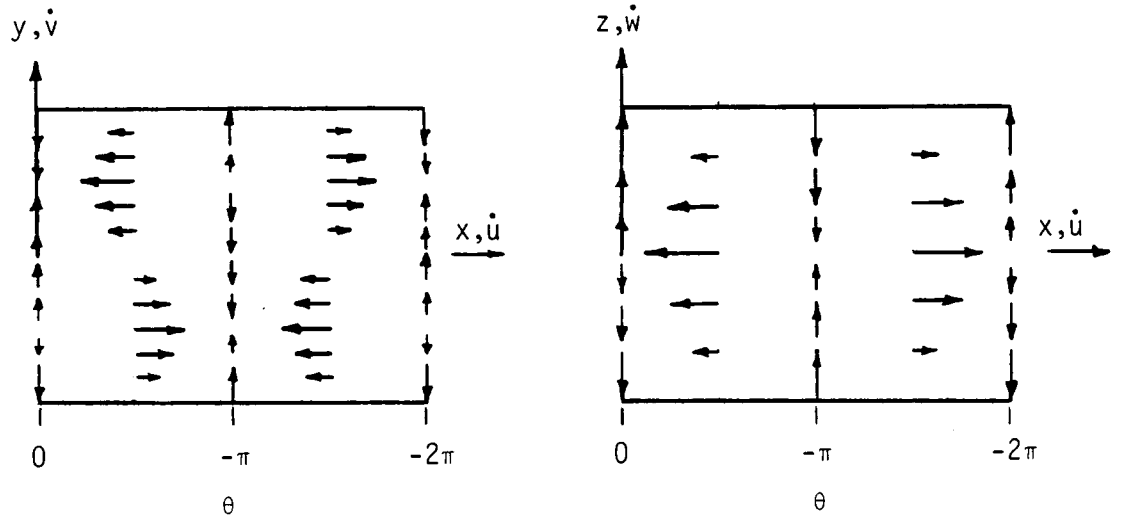
$$H_B = \int_{-c/2}^{c/2} \tau_{zy}\Big|_{z=-g/2} dy , \tag{4.21a}$$

$$H_T = \int_{-c/2}^{c/2} \tau_{zy}\Big|_{z=g/2} dy , \tag{4.21b}$$

$$V_B = \int_{-c/2}^{c/2} -\sigma_{zz}\Big|_{z=-g/2} dy , \tag{4.21c}$$



(a)



(b)

Figure 4.6. Fluid Flow Patterns Due to Rotation. Length of θ is $2\pi/\lambda$, the Period of the Phase, y is from c/2 to -c/2, and z is From g/2 to -g/2. Patterns Are For (a) Opening or Closing of the Gap, and (b) Rigid Body Displacement of the Gap.

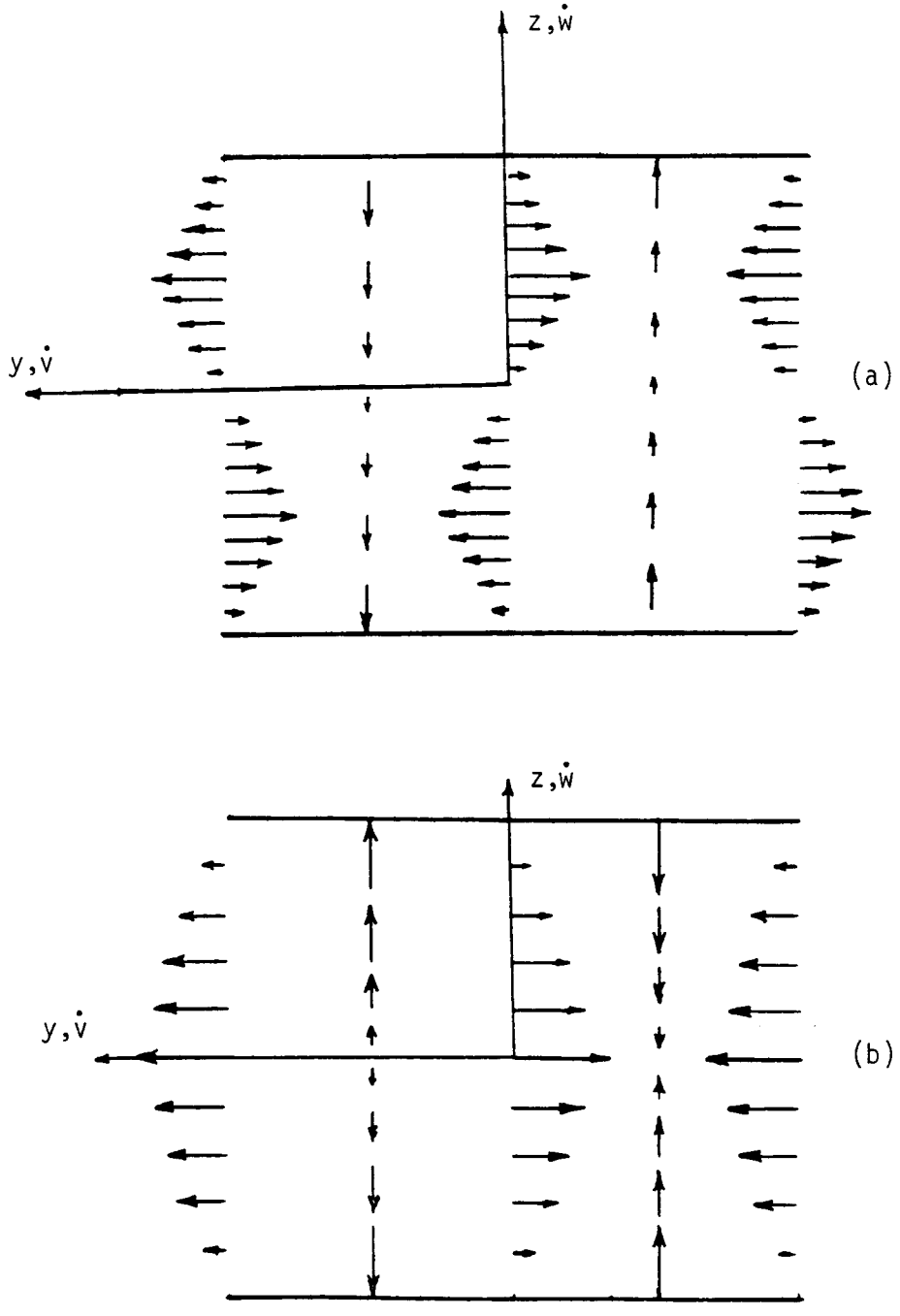


Figure 4.7. Fluid Flow in the yz Plane Due to Rotation. Bounds on y and z are ±c/2 and ±g/2, Respectively. Patterns are For (a) Opening or Closing of the Gap, and (b) Rigid Body Displacement of the Gap.

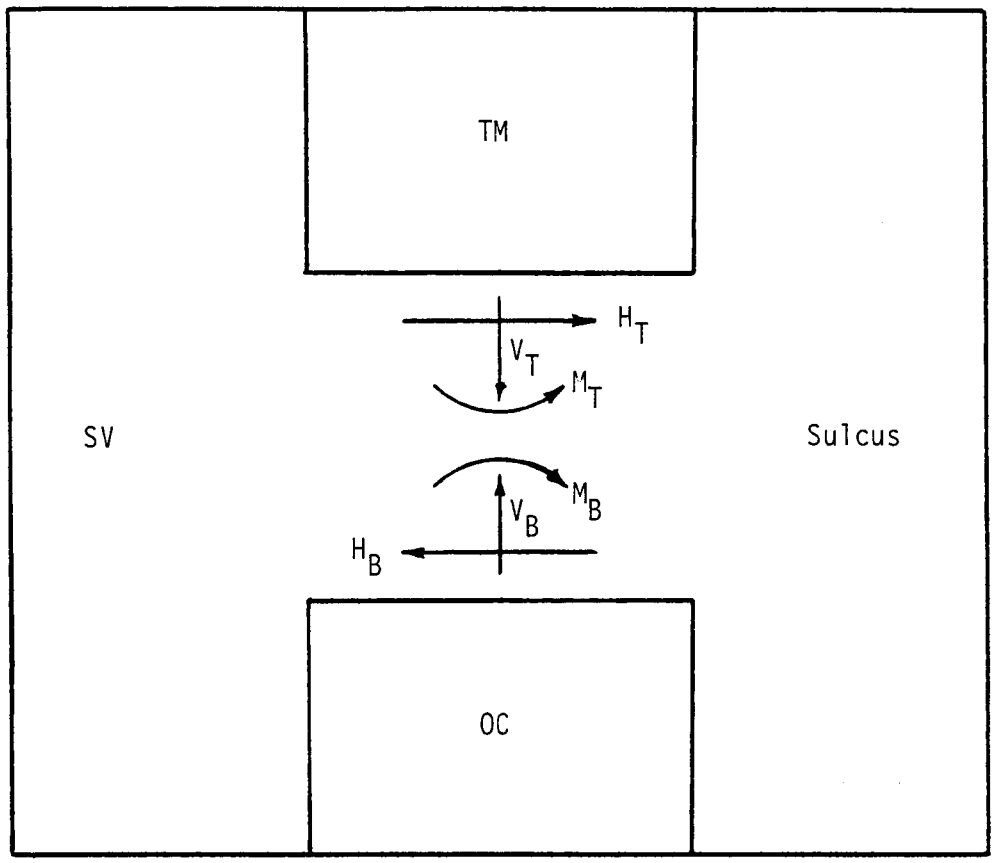


Figure 4.8. Resistive Fluid Forces on the Organ of Corti and Tectorial Membrane Beams. The Spring Stiffness Coefficients Associated with the "Potential Energy" of the "Fluid Springs" are Derived From These.

$$V_T = \int_{-c/2}^{c/2} -\sigma_{zz}\Big|_{z=g/2} dy \ , \tag{4.21d}$$

$$M_B = \int_{-c/2}^{c/2} -\sigma_{zz}\Big|_{z=-g/2} ydy \ , \tag{4.21e}$$

$$M_T = \int_{-c/2}^{c/2} -\sigma_{zz}\Big|_{z=g/2} ydy \ , \tag{4.21f}$$

where

$$\sigma_{zz} = -p + 2\mu \frac{\partial \dot{w}}{\partial z} \tag{4.21g}$$

$$\tau_{zy} = \mu\left(\frac{\partial \dot{v}}{\partial z} + \frac{\partial \dot{w}}{\partial y}\right) \ . \tag{4.21h}$$

To determine the resisting fluid forces, we substitute the expressions for the velocity and pressure fields for each of the block displacements into Eqs. (4.21). For horizontal displacement,

$$H_B = \frac{\beta\mu c}{2}\left[(a_B\dot{\chi}_B + a_T\dot{\chi}_T)\tanh\gamma + \frac{(a_B\dot{\chi}_B - a_T\dot{\chi}_T)}{\tanh\gamma}\right] \ , \tag{4.22a}$$

$$H_T = \frac{\beta\mu c}{2}\left[-(a_B\dot{\chi}_B + a_T\dot{\chi}_T)\tanh\gamma + \frac{(a_B\dot{\chi}_B - a_T\dot{\chi}_T)}{\tanh\gamma}\right] \ , \tag{4.22b}$$

$$V_B = V_T = 0 \ , \tag{4.22c}$$

and

$$M_B = M_T = 0 \ , \tag{4.22d}$$

where β and γ are given by Eqs. (4.6c) and (4.9f), respectively. For vertical displacement,

$$H_B = H_T = 0 \ , \tag{4.23a}$$

$$V_B = \frac{4i\rho\omega}{c} \sum_{j=0}^{\infty} \frac{\beta_j}{\alpha_j^2 m_j} \left[(\dot{\delta}_T + \dot{\delta}_B) TM1_j - (\dot{\delta}_T - \dot{\delta}_B) TM2_j \right] \ , \tag{4.23b}$$

$$V_T = \frac{-4i\rho\omega}{c} \sum_{j=0}^{\infty} \frac{\beta_j}{\alpha_j^2 m_j} \left[(\dot{\delta}_T + \dot{\delta}_B) TM1_j + (\dot{\delta}_T - \dot{\delta}_B) TM2_j \right] \ , \tag{4.23c}$$

and

$$M_B = M_T = 0 \ , \tag{4.23d}$$

where

$$\alpha_j = (2j + 1) \frac{\pi}{c} \ , \tag{4.23e}$$

$$TM1_j = \frac{\tanh \gamma_j \tanh \eta_j}{\beta_j \tanh \gamma_j - m_j \tanh \eta_j} \ , \tag{4.23f}$$

$$TM2_j = \frac{1}{\beta_j \tanh \eta_j - m_j \tanh \gamma_j} \ , \tag{4.23g}$$

and β_j, γ_j, η_j, and m_j are defined in Eqs. (4.16). For the rotational displacement,

$$H_B = H_T = 0 \ , \tag{4.24a}$$

$$V_B = V_T = 0 \ , \tag{4.24b}$$

$$M_B = i\rho\omega c \sum_{j=0}^{\infty} \frac{\beta_j}{m_j \alpha_j^2} \left[(\dot{\chi}_B + \dot{\chi}_T) TM2_j + (\dot{\chi}_B - \dot{\chi}_T) TM1_j \right] , \quad (4.24c)$$

and

$$M_T = i\rho\omega c \sum_{j=0}^{\infty} \frac{\beta_j}{m_j \alpha_j^2} \left[(\dot{\chi}_B + \dot{\chi}_T) TM2_j - (\dot{\chi}_B - \dot{\chi}_T) TM1_j \right] , \quad (4.24d)$$

where

$$\alpha_j = \frac{2\pi}{c} (j + 1) . \quad (4.24e)$$

To determine the spring stiffnesses associated with these fluid forces, we first consider a simple spring-mass-damper system with harmonic excitation as illustrated in Figure 4.9. Lagrange's equation for the system is

$$\frac{d}{dt} \left(\frac{\partial T}{\partial \dot{x}} \right) - \frac{\partial T}{\partial x} + \frac{\partial U}{\partial x} = Q , \quad (4.25a)$$

where

$$Q = \frac{\delta W}{\delta x} , \quad (4.25b)$$

and U and T are the potential energy and kinetic energy of the system, respectively. The virtual work, δW, done by all but the inertia and conservative forces is included in Q. For the system shown in Figure 4.9, we can write

$$T = m\dot{x}^2/2 , \quad (4.26a)$$

$$U = kx^2/2 , \quad (4.26b)$$

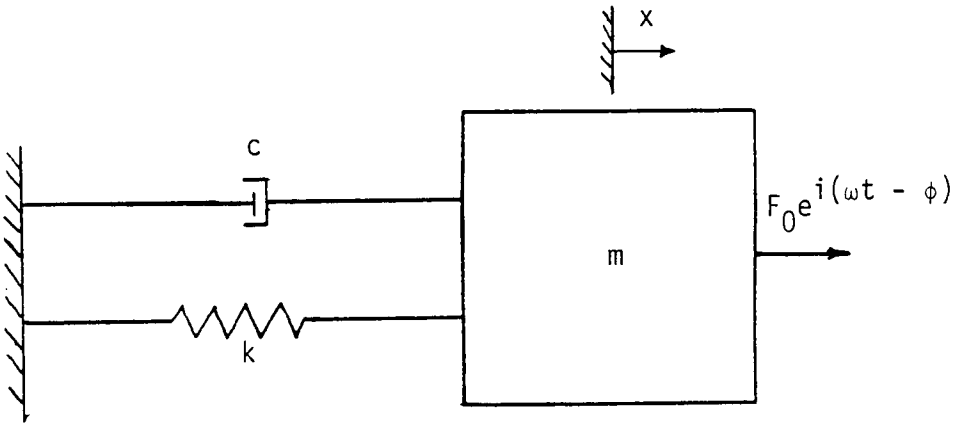


Figure 4.9. Spring-Mass-Damper System with Harmonic Excitation.

$$\delta W = -c\dot{x}\delta x + F_0 e^{i(\omega t - \phi)}\delta x \ , \tag{4.26c}$$

$$Q_x = -c\dot{x} + F_0 e^{i(\omega t - \phi)} \ . \tag{4.26d}$$

Using

$$x = Xe^{i(\omega t - \phi)} \ , \tag{4.27}$$

in Eqs. (4.25) and (4.26), we get

$$(-m\omega^2 + k + i\omega c)x = F_0 e^{i(\omega t - \phi)} \ . \tag{4.28}$$

However, for this system, we can also write

$$T = 0 \ , \tag{4.29a}$$

$$U = \frac{1}{2}(k - m\omega^2 + i\omega c)x^2 \ , \tag{4.29b}$$

$$\delta W = F_0 e^{i(\omega t - \phi)}\delta x \ , \tag{4.29c}$$

$$Q_x = F_0 e^{i(\omega t - \phi)} \ . \tag{4.29d}$$

From Eqs. (4.25), (4.27) and (4.29), we obtain

$$(k - m\omega^2 + i\omega c)x = F_0 e^{i(\omega t - \phi)} \ , \tag{4.30}$$

which is the same as the solution given by Eq. (4.28). Therefore, for harmonic excitation and response, we can incorporate any mechanical effect in the stiffness matrix.

For the gap flow models, the generalized forces are

$$Q_{\chi_B} = M_B - a_B H_B \ , \tag{4.31a}$$

$$Q_{\delta_B} = V_B \ , \tag{4.31b}$$

$$Q_{\chi_T} = M_T + a_T H_T \ , \tag{4.31c}$$

$$Q_{\delta_T} = -V_T \tag{4.31d}$$

Equations (4.31) can be written in matrix form as

$$\{Q_i\} = [Q]\{\dot{u}_i\} \ , \tag{4.32a}$$

where

$$\{\dot{u}_i\} = \{\dot{\chi}_B, \ \dot{\delta}_B, \ \dot{\chi}_T, \ \dot{\delta}_T\}^T \ , \tag{4.32b}$$

and [Q] is a matrix of order four. For harmonic excitation, we see from Eq. (4.27) that

$$\{\dot{u}_i\} = i\omega\{u_i\} \ . \tag{4.33}$$

Thus, from Eqs. (4.32) and (4.33), we have

$$\{Q_i\} = i\omega[Q]\{u_i\} \ . \tag{4.34}$$

When these generalized forces are moved to the left-hand side of Lagrange's equation the equivalent stiffness, $[K_T]$, becomes

$$[K_T] = -i\omega[Q] \tag{4.35}$$

Using Eqs. (4.22), (4.23), (4.24), (4.31) and (4.32), we find that Eq. (4.35) can be written as

$$[K_T] = \begin{pmatrix} k_R p + a_B^2 k_H p & 0 & k_R m + a_B a_T k_H m & 0 \\ 0 & k_V p & 0 & k_V m \\ k_R m + a_B a_T k_H m & 0 & k_R p + a_T^2 k_H p & 0 \\ 0 & k_V m & 0 & k_V p \end{pmatrix}, \tag{4.36a}$$

where

$$k_H p = \frac{i\omega c \mu \beta}{2} (\tanh \gamma + \coth \gamma), \tag{4.36b}$$

$$k_H m = \frac{i\omega c \mu \beta}{2} (\tanh \gamma - \coth \gamma), \tag{4.36c}$$

$$k_V p = \frac{4\rho\omega^2}{c} \sum_{j=0}^{\infty} \frac{\beta_j}{m_j \alpha_{vj}^2} (TM1_j + TM2_j), \tag{4.36d}$$

$$k_V m = \frac{4\rho\omega^2}{2} \sum_{j=0}^{\infty} \frac{\beta_j}{m_j \alpha_{vj}^2} (TM1_j - TM2_j), \tag{4.36e}$$

$$k_R p = \rho\omega^2 c \sum_{j=0}^{\infty} \frac{\beta_j}{m_j \alpha_{rj}^2} (TM1_j + TM2_j), \tag{4.36f}$$

$$k_R m = \rho\omega^2 c \sum_{j=0}^{\infty} \frac{\beta_j}{m_j \alpha_{rj}^2} (TM2_j - TM1_j), \tag{4.36g}$$

$$\alpha_{vj} = (2j + 1) \frac{\pi}{c}, \tag{4.36h}$$

$$\alpha_{rj} = 2(j + 1)\,\frac{\pi}{c}\,, \tag{4.36i}$$

and β, γ, β_j, and m_j are given by Eqs. (4.6c), (4.9f), (4.16o), and (4.16p), respectively. The corresponding stiffness matrix for the two-dimensional model is

$$[K_D] = \begin{bmatrix} k_R + a_B^2 k_H p & 0 & k_R + a_B a_T k_H m & 0 \\ 0 & k_V & 0 & -k_V \\ k_R + a_B a_T k_H m & 0 & k_R + a_T^2 k_H p & 0 \\ 0 & -k_V & 0 & k_V \end{bmatrix}, \tag{4.37a}$$

where

$$k_V = i\omega\mu \left(\frac{c}{g}\right)^3 \frac{\gamma^3}{3(\gamma - \tanh \gamma)}\,, \tag{4.37b}$$

$$k_R = i\omega\mu \left(\frac{c^5}{g^3}\right) S_R\,, \tag{4.37c}$$

$$S_R = \frac{3}{4\pi^4} \sum_{j=1}^{\infty} \frac{1}{j^4} \frac{\gamma_j^3}{3(\gamma_j - \tanh \gamma_j)}\,, \tag{4.37d}$$

and γ_j is given by Eq. (4.16m). It can be shown that Eqs. (4.36d) and (4.36f) reduce to Eqs. (4.37b) and (4.37c), respectively, when the wavenumber vanishes and

$$\tanh \eta_j = \eta_j\,, \tag{4.38}$$

where η_j is given by Eq. (4.16n). This approximation is appropriate whenever $\eta_j \lesssim 0.3$. Since η_j is proportional to the gap height, Eq. (4.16n), the gap height can be small enough so that Eq. (4.38) holds for some finite number of terms in Eqs. (4.36d) and (4.36f). But because η_j is also proportional to j, Eq. (4.38) eventually breaks down no matter how small the gap height. Nevertheless, if the gap height is small enough, the breakdown of Eq. (4.38) is postponed until the terms in the series are so small as to be irrelevant. For a gap height in this range and wavenumber sufficiently small, the three-dimensional spring stiffnesses would differ negligibly from the two-dimensional stiffnesses. In this case, we would expect terms proportional to $TM1_j$ [see Eqs. (4.36d) and (4.36f)], to be much smaller than the terms proportional to $TM2_j$, which correspond directly to the two-dimensional stiffnesses.

5. SYSTEM ENERGY

5.1. Partition Energy

Using the system coordinates defined in Figure 4.3, p. 20, we can write the potential energy of the partition as

$$U_p = (1/2)\{u\}^T[K]\{u\} \ , \tag{5.1a}$$

where

$$\{u\} = \begin{Bmatrix} \eta_1 \\ \eta_2 \\ \eta_3 \\ x_B \\ \delta_B \\ x_T \\ \delta_T \end{Bmatrix} \ . \tag{5.1b}$$

By applying the principle of stationary potential, Boulet has shown that Eq. (5.1a) can be changed to

$$U_p = (1/2)\{p\}^T_{z=0}\,[C]\{p\}_{z=0} \ , \tag{5.2a}$$

where

$$\{p\} = \begin{Bmatrix} p_1 \\ p_2 \\ p_3 \end{Bmatrix} \ , \tag{5.2b}$$

$$[C] = [F]^T[S] \,, \tag{5.2c}$$

$$[F] = [K]^{-1}[S] \,, \tag{5.2d}$$

$$[S] = \begin{bmatrix} -b_1 & b_1 & 0 \\ 0 & b_2 & -b_2 \\ -b_3 & 0 & b_3 \\ S_{41} & S_{42} & S_{43} \\ S_{51} & S_{52} & S_{53} \\ S_{61} & S_{62} & S_{63} \\ S_{71} & S_{72} & S_{73} \end{bmatrix} \,, \tag{5.2e}$$

$$S_{41} = \frac{1}{2}\left(a_B^2 - \frac{1}{6}c^2 + ga_B\frac{\tanh\gamma}{\gamma} - \frac{1}{2}b_1(c + \frac{1}{3}b_1)\right) \,, \tag{5.2f}$$

$$S_{42} = \frac{1}{4}\left(b_1(c + \frac{1}{3}b_1) - b_2(c + \frac{1}{3}b_2)\right) \,, \tag{5.2g}$$

$$S_{43} = \frac{1}{2}\left(\frac{1}{2}b_2(c + \frac{1}{3}b_2) - a_B^2 + \frac{1}{6}c^2 - ga_B\frac{\tanh\gamma}{\gamma}\right) \,, \tag{5.2h}$$

$$S_{51} = -\frac{1}{2}(b_1 + c) \,, \tag{5.2i}$$

$$S_{52} = \frac{1}{2}(b_1 + b_2 + 2c) \,, \tag{5.2j}$$

$$S_{53} = -\frac{1}{2}(b_2 + c) \,, \tag{5.2k}$$

$$S_{61} = \frac{1}{2}\left(a_T^2 - \frac{1}{6}c^2 + ga_T\frac{\tanh\gamma}{\gamma} - \frac{1}{2}b_3(c + \frac{1}{3}b_3)\right) \,, \tag{5.2l}$$

$$S_{62} = 0 \ , \tag{5.2m}$$

$$S_{63} = -S_{61} \ , \tag{5.2n}$$

$$S_{71} = -\frac{1}{2}(b_3 + c) \ , \tag{5.2o}$$

$$S_{72} = 0 \ , \tag{5.2p}$$

$$S_{73} = \frac{1}{2}(b_3 + c) \ . \tag{5.2q}$$

The dimensions a_B, a_T, c, b_1, b_2, and b_3 are defined in Figure 1.2 (p. 4), γ is defined in Eq. (4.9f), and p_1, p_2, and p_3 are the fluid pressures in scala vestibuli, scala tympani, and the inner sulcus, respectively.

The various contributions to the potential energy of the partition include the elastic strain energies associated with displacement of the membranes, the elastic strain energies due to longitudinal bending and twisting of the beams, the kinetic energy associated with the inertia of the beams and the "potential energy" of the "fluid springs." To account for these contributions, we write the stiffness matrix of the system as

$$[K] = [K_M] + [K_B] + [K_S] - [G_B] \ , \tag{5.3}$$

where the matrices, $[K_M]$, $[K_B]$, $[K_S]$, and $[G_B]$, are associated with the potential energy of the membranes, the potential energy of the beams, the "potential energy" of the "fluid springs" and the kinetic energy of the beams, respectively. The "fluid springs" stiffness

matrix accounts for both the damping and inertia of the gap fluid and can be written as

$$[K_S] = \left[\begin{array}{c|cccc} \begin{matrix}3\\3[0]\end{matrix} & \multicolumn{4}{c}{\begin{matrix}4\\3[0]\end{matrix}} \\ \hline \begin{matrix}\\3\\4[0]\\\end{matrix} & \begin{matrix} k_R p + a_B^2 k_H p & 0 & k_R m + a_B a_T k_H p & 0 \\ 0 & k_V p & 0 & k_V m \\ k_R m + a_B a_T k_H p & 0 & k_R p + a_T^2 k_H p & 0 \\ 0 & k_V m & 0 & k_V p \end{matrix} \end{array}\right], \tag{5.4}$$

where $k_H p$, $k_H m$, $k_V p$, $k_V m$, $k_R p$, and $k_R m$ are given by Eqs. (4.36). Boulet has shown that

$$[K_M] = 720 \begin{bmatrix} \dfrac{D_{y1}}{b_1^3} & 0 & 0 \\ 0 & \dfrac{D_{y2}}{b_2^3} & 0 \\ 0 & 0 & \dfrac{D_{y3}}{b_3^3} \end{bmatrix}, \tag{5.5a}$$

$$[K_B] = \left[\begin{array}{c|cccc} \begin{matrix}3\\3[0]\end{matrix} & \multicolumn{4}{c}{\begin{matrix}4\\3[0]\end{matrix}} \\ \hline \begin{matrix}\\3\\4[0]\\\end{matrix} & \begin{matrix} \lambda^2 (GJ)_B & 0 & 0 & 0 \\ 0 & \lambda^4 (EI)_B & 0 & 0 \\ 0 & 0 & \lambda^2 (GJ)_T & 0 \\ 0 & 0 & 0 & \lambda^4 (EI)_T \end{matrix} \end{array}\right], \tag{5.5b}$$

$$[G_B] = \omega^2[M] \ , \tag{5.5c}$$

where

$$D_{yj} = \frac{E_j h_j^3}{12} \tag{5.5d}$$

E = Young's modulus for the beam,

G = shear modulus,

h_j = membrane thickness,

b_j = membrane width,

J = geometrical property of the cross section shape,

I = second moment of the beam cross section per unit length in the x-direction,

$$[M] = \left(\begin{array}{c|cccc} \overset{3}{3}[0] & \multicolumn{4}{c}{\overset{4}{3}[0]} \\ \hline & \frac{1}{12} M_B(4a_B^2 + c) & 0 & 0 & 0 \\ & 0 & M_B & 0 & 0 \\ \overset{3}{4}[0] & 0 & 0 & \frac{1}{12} M_T(4a_T^2 + c) & 0 \\ & 0 & 0 & 0 & M_T \end{array}\right), \tag{5.5e}$$

M_B = organ of Corti block mass per unit length in the x-direction,

M_T = tectorial membrane block mass per unit length in the x-direction,

and a_B, a_T, and c are the dimensions shown in Figure 1.2, p. 4.

5.2. Gap Flow Inertia

The three-dimensional gap flow inertia matrix is easily established from Eqs. (4.12a) and (3.3c) as being

$$[G_G] = S_1 \begin{pmatrix} 1 & 0 & 1 \\ 0 & 0 & 0 \\ 1 & 0 & 1 \end{pmatrix} + S_2 \begin{pmatrix} 1 & 0 & -1 \\ 0 & 0 & 0 \\ -1 & 0 & 1 \end{pmatrix} \tag{5.6}$$

where S_1 and S_2 are defined by Eqs. (4.12).

5.3. Duct Flow Inertia

The duct flow inertia matrix for the present model is the same as the one derived by Boulet (1984) for two-dimensional duct flow, and is written as

$$[G] = \begin{pmatrix} G_1 & 0 & 0 \\ 0 & G_1 & 0 \\ 0 & 0 & G_3 \end{pmatrix} , \tag{5.7a}$$

where

$$G_1 = \frac{L_1}{\rho\omega^2 H_{eq}} , \tag{5.7b}$$

$$G_3 = \frac{b_3}{\rho\omega^2 H_3} , \tag{5.7c}$$

$$H_{eq} = \frac{L_2}{\xi \tanh \xi}\left(1 + \frac{\xi(2 - \tanh^2 \xi)}{\zeta \tanh \xi}\right) , \tag{5.7d}$$

$$H_3 = \frac{L_1^2}{2L_3\xi^2}\left(1 + \frac{3L_2}{\zeta b_3}\right), \tag{5.7e}$$

$$\zeta = \beta L_2 , \tag{5.7f}$$

and ξ and β are given by Eqs. (3.8e) and (4.6c), respectively, and the dimensions L_1, L_2, L_3, and b_3 are shown in Figure 1.2, p. 4. G_1, G_2, and G_3 account for fluid kinetic energy in scala vestibuli, scala tympani, and the inner sulcus, respectively.

6. DISPERSION RELATION

In Section 3 the dispersion relation.

$$|D| = 0 \ , \tag{6.1}$$

was found from the time-averaged Lagrangian and the eikonal equation. Using Eqs. (3.5), (5.2), (5.6), (5.7), and (6.1), we can write the dispersion relation as

$$\begin{aligned} G_3[G_1^2 &+ (S_1 + S_2 - \tau)G_1 - (S_1 + S_2)C_{22} + \delta] \\ &+ (S_1 + S_2 - \sigma)G_1^2 + 2G_1\delta - 2G_1C_{22}S_2 \\ &+ [4(G_1 - C_{22})S_2 + 4\delta - 2(C_{11} + \sigma)G_1]S_1 = 0 \ , \end{aligned} \tag{6.2a}$$

where

$$\tau = C_{11} + C_{22} \ , \tag{6.2b}$$

$$\delta = C_{11}C_{22} - C_{12} \ , \tag{6.2c}$$

$$\sigma = C_{11} + 2C_{12} + C_{22} \ , \tag{6.2d}$$

and G_1, G_3, S_1, and S_2 are given by Eqs. (5.7b), (5.7c), (4.12b), and (4.12c), respectively. Equation (6.2a) can also be written as

$$\begin{aligned} s^2 &- \{(1 - r_c) + q(r_1 - r_c)\}s + (1 + 2q)(r_2 - r_c r_3) \\ &+ 4qr_f(r_g - r_4) + \frac{4qr_f(r_2 - r_3 r_g)}{s} = 0 \ , \end{aligned} \tag{6.3a}$$

where

$$s = \frac{L_1 \xi \tanh \xi}{\rho\omega^2 \tau L_2 (1 + a_1)} , \tag{6.3b}$$

$$q = \frac{L_1 \tanh \xi (1 + a_3)}{\varepsilon \xi L_2} , \tag{6.3c}$$

$$r_1 = \frac{\sigma}{\tau} , \tag{6.3d}$$

$$r_2 = \frac{\delta}{\tau^2} , \tag{6.3e}$$

$$r_3 = \frac{C_{22}}{\tau} , \tag{6.3f}$$

$$r_4 = \frac{(C_{11} + C_{12})}{\tau} , \tag{6.3g}$$

$$r_f = \frac{S_1}{\tau} , \tag{6.3h}$$

$$r_g = \frac{S_2}{\tau} , \tag{6.3i}$$

$$r_c = r_f + r_g , \tag{6.3j}$$

$$a_1 = \frac{\xi(2 - \tanh^2 \xi)}{\zeta \tanh \xi} , \tag{6.3k}$$

$$a_3 = \frac{3L_2}{b_3\zeta} , \tag{6.3l}$$

$$\varepsilon = \frac{2b_3L_3}{L_2^2} , \tag{6.3m}$$

and ξ and ζ are given by Eqs. (3.8e) and (5.7f), respectively, and the dimensions L_1, L_2, L_3, and b_3 are shown in Figure 1.2, p. 4.

The dispersion relation defined by Eq. (6.3a) has two nontrivial roots, each of which corresponds to a propagating wave. The propagating wave associated with the smaller root will be referred to as mode 1, while the propagating wave associated with the larger root will be referred to as mode 2. For each mode there are two complex roots equal in magnitude but opposite in sign. The root with a negative real part corresponds to a wave traveling in the negative x direction and is of no interest since waves are initiated at the stapes (x = 0) and propagate only in the positive x direction. The remaining root of each mode has a negative imaginary part which corresponds to a wave whose amplitude decreases with x. Since the imaginary part of the root causes the wave to decay, it corresponds to damping in the system.

The complex roots of the dispersion relation, Eq. (6.3a), are determined using Muller's method [Conte and De Boor (1972)].

7. DATA

The quantitative data used in the simulation are taken from Helle (1974) with the exception of gap height. In the present study, the gap height varies from 0.01 mm at the stapes to 0.41 mm at $x = 1000$ mm. All data from Helle's model G2 (see Figure 1.2, p. 4) are given in Tables 7.1 and 7.2.

Table 7.1. Geometrical Data for Three-Dimensional Simulation

Dimension	Length
L_1	35
L_2	35
h_1	0.5
h_2	0.5
h_3	1.0
a_B	3.5
a_T	4.0
g	$1.0 \times 10^{-2} + 4.0 \times 10^{-4}x$
L_3	$(a_B + a_T + g)/2.0$
c	$2.0 + 3.0 \times 10^{-3}x$
b_2	$1.0 + 1.6 \times 10^{-3}x$
b_3	$3.0 + 4.6 \times 10^{-3}x$
d	$5.0 + 5.6 \times 10^{-3}x$, $0 < x < 250$ $6.4 + 7.2 \times 10^{-3}(x - 250)$, $250 < x < 500$ $8.2 + 9.6 \times 10^{-3}(x - 500)$, $500 < x < 750$ $10.6 + 12.0 \times 10^{-3}(x - 750)$, $750 < x < 1000$
b_1	$d - c - b_2$

All data except gap height are taken from Helle (1974). All dimensions are given in millimeters.

Table 7.2. Mechanical Data for Three-Dimensional Simulation

Property	Value
E_1 (N/mm^2)	0.65 (1 + 0.04i)
E_2 (N/mm^2)	0.65 (1 + 0.04i)
E_3 (N/mm^2)	0.30 (1 + 0.035i)
μ ($N \cdot s/mm^2$)	27×10^{-9}
ρ_B ($N \cdot s^2/mm^4$)	1.09×10^{-9}
ρ_T ($N \cdot s^2/mm^4$)	0.94×10^{-9}
ρ ($N \cdot s^2/mm^4$)	1.15×10^{-9}

All data are taken from Helle (1974).

8. RESULTS

Results of the present study are presented below in two parts:

1. Stiffness terms,
2. Wavenumbers.

Because there are no interesting changes from two-dimensional results, no further comparisons were performed.

8.1. Stiffness Terms

Gap flow spring stiffnesses for the two models are shown in Figures 8.1 and 8.2. The three-dimensional model stiffnesses are almost identical to the stiffnesses of the two-dimensional model. These curves indicate that, as discussed in Section 4.4, the gap height and wavenumbers for Helle's G2 are small enough so that the two-dimensional spring stiffnesses are accurate.

The amount of damping in the springs is proportional to their imaginary parts, and is found to decrease rapidly with x (see Figures 8.3 and 8.4). Thus, for small gap heights the inertia of the gap fluid is small compared to the amount of damping associated with the springs. For larger gap heights, the gap flow inertia becomes of the same magnitude as the damping. However, at no position does the damping become insignificant. The viscous boundary layer thickness for both models can be found from

$$\delta = \frac{\pi}{Re\beta} , \tag{8.1}$$

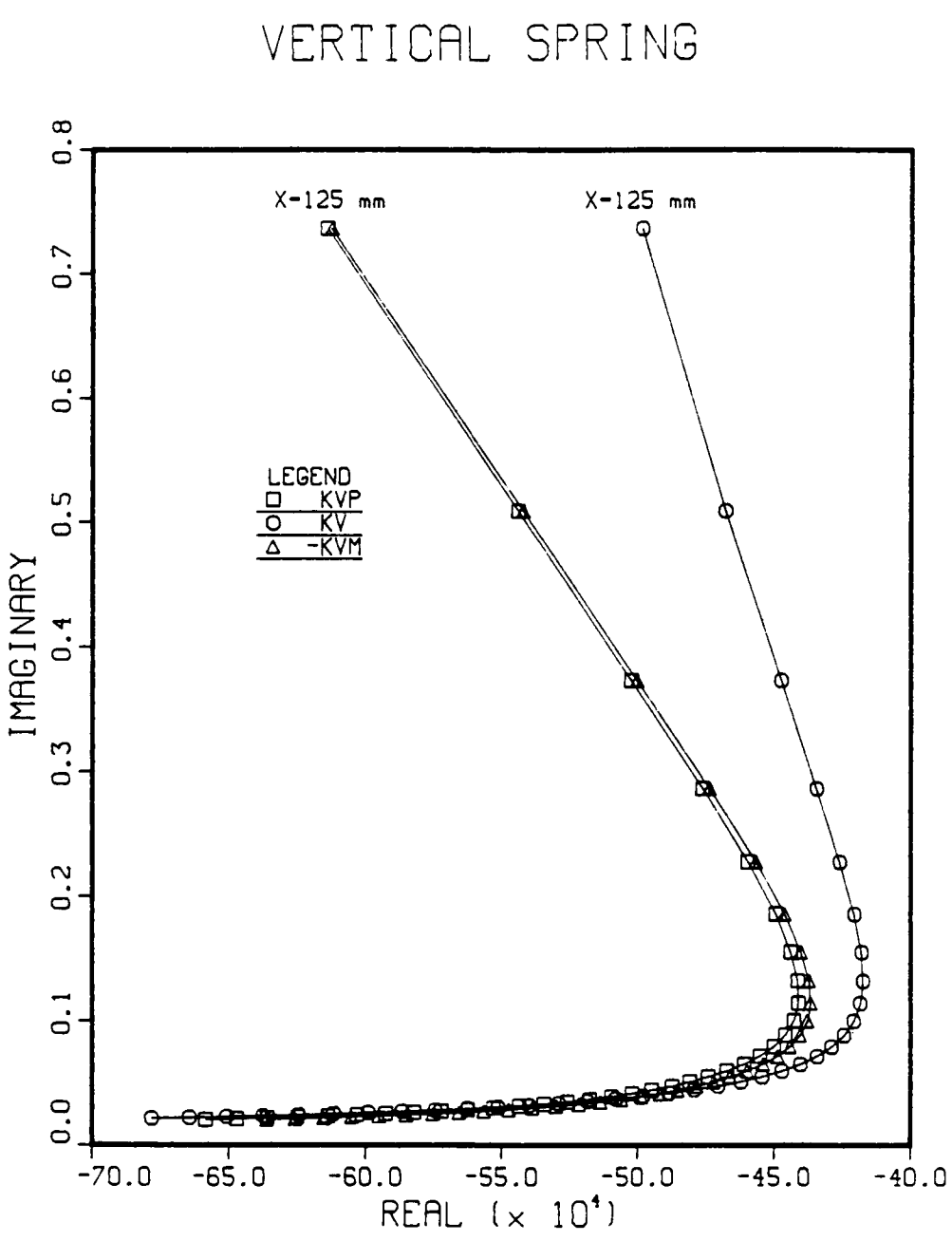


Figure 8.1. Imaginary vs. Real, Complex Vertical Spring Stiffness, 70 Hz. Distance From Stapes Varies From 125 mm to 1000 mm at 25 mm Increments. Damping in Three-Dimensional Model is the Same as the Two-Dimensional Model.

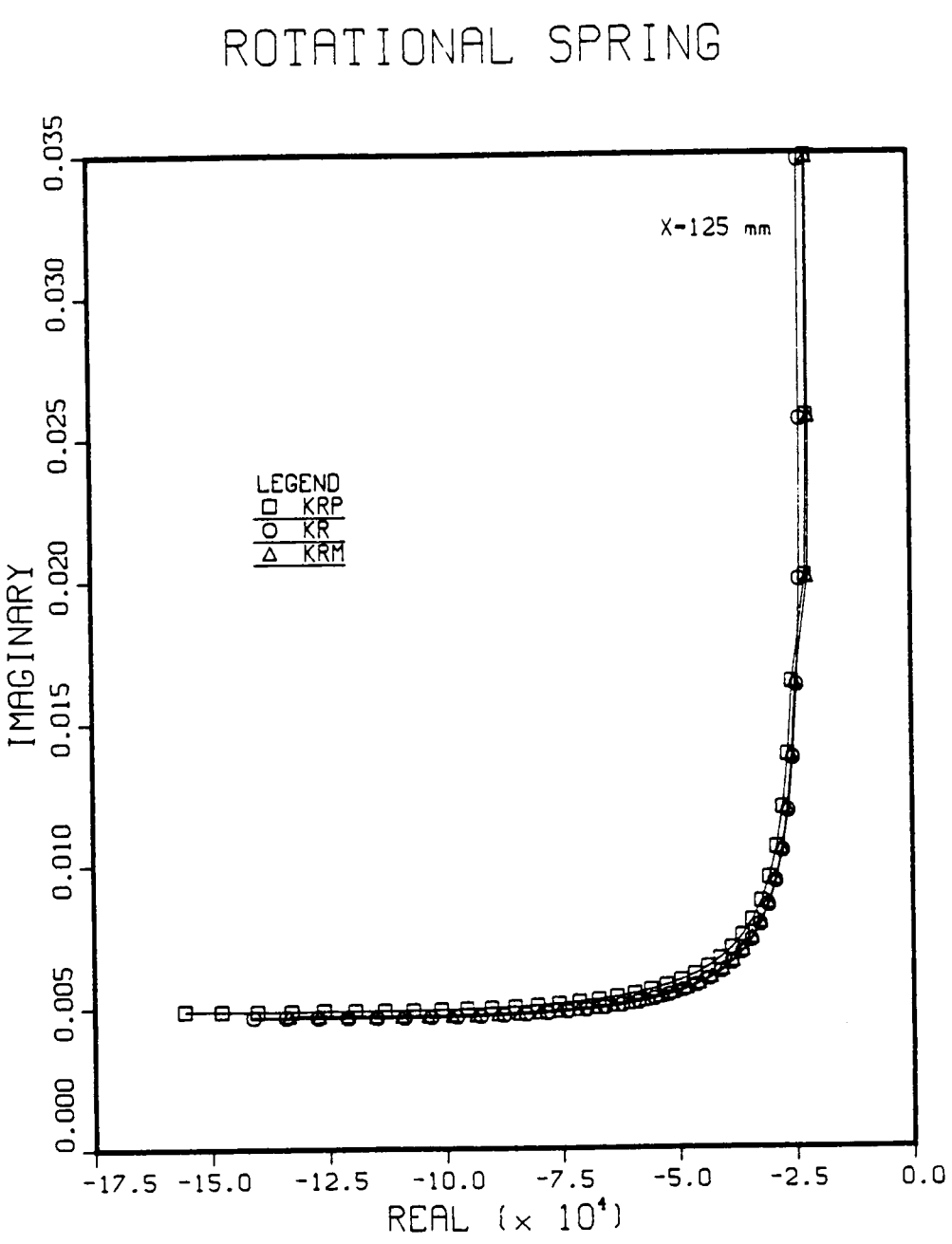


Figure 8.2. Imaginary vs. Real, Complex Rotational Spring Stiffness, 70 Hz. Distance From the Stapes Varies From 125 mm to 1000 mm at 25 mm Increments. Damping From Rotational Spring is the Same in Both the Two-Dimensional and the Three-Dimensional Models.

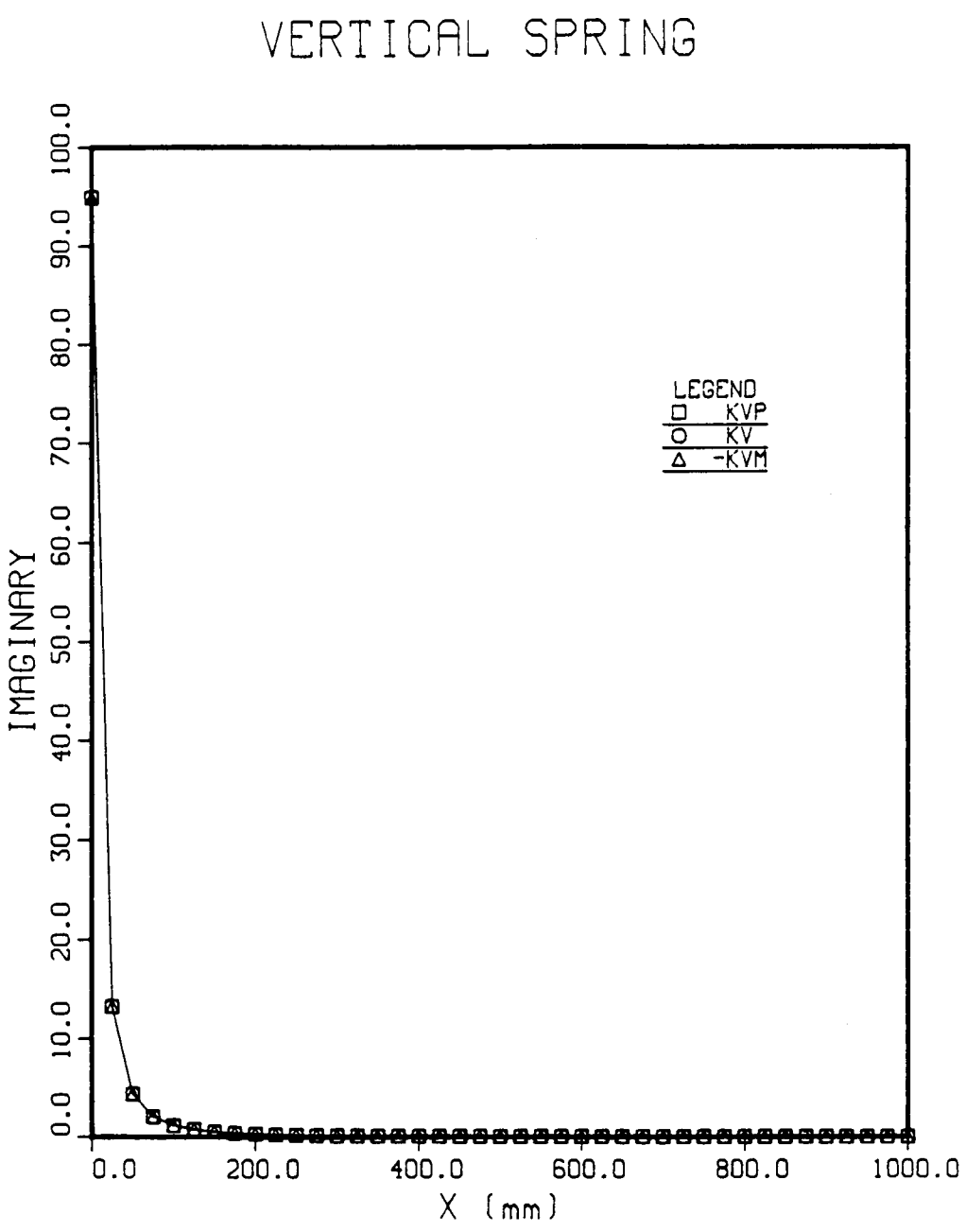


Figure 8.3. Vertical Spring Stiffness vs. Distance From Stapes, 70 Hz. Vertical Spring Damping Decreases Rapidly With Distance From Stapes for Both the Two-Dimensional and the Three-Dimensional Models.

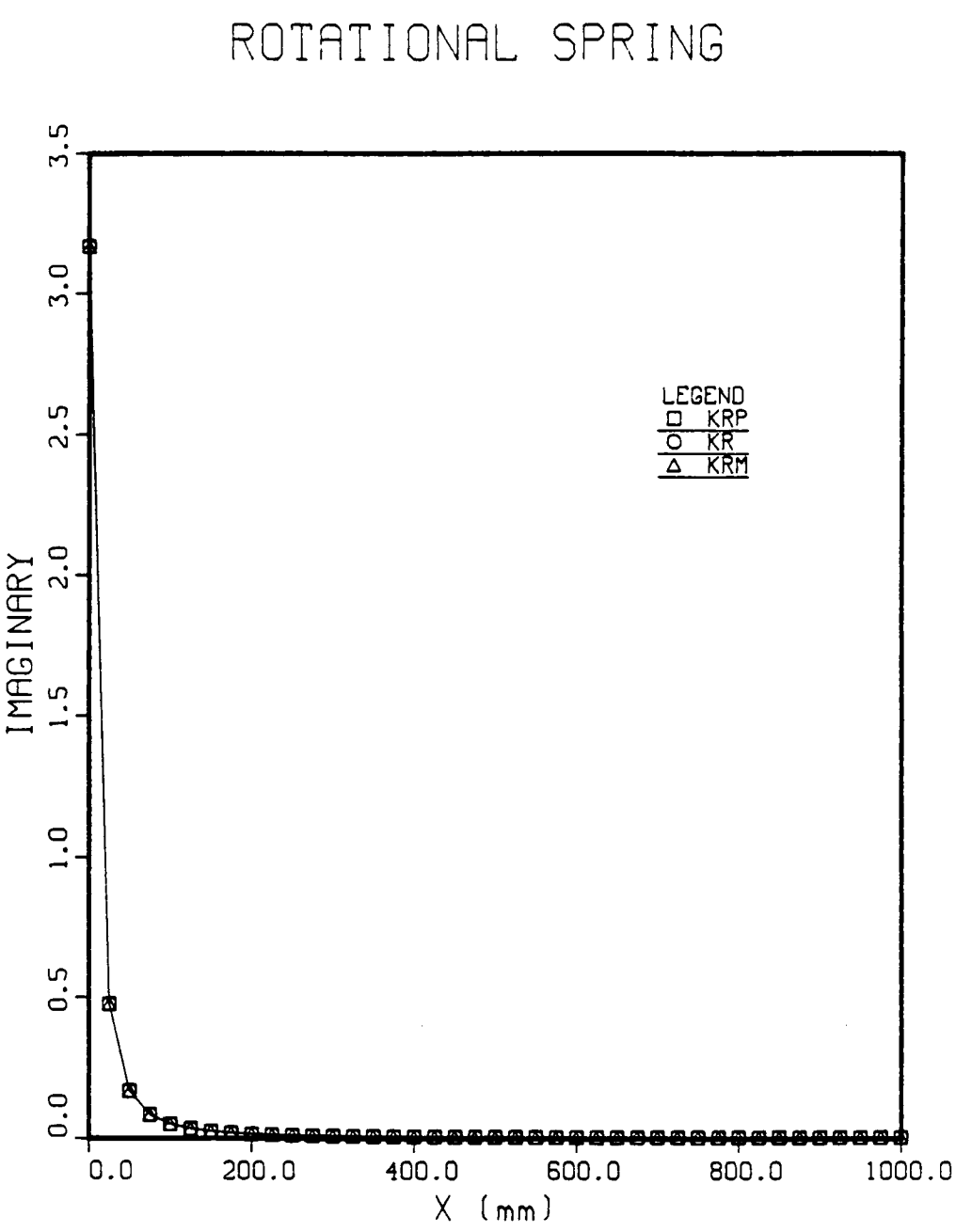


Figure 8.4. Rotational Spring Stiffness vs. Distance From Stapes, 70 Hz. Damping Due to Rotational Spring Decreases Rapidly With Distance From Stapes in Each Model.

and is approximately 1 mm. This value is larger than the maximum gap height of 0.41 mm. Thus, the gap is completely filled with boundary layer for all x.

8.2. Wavenumbers

For the three-dimensional model the dispersion relation from Section 6 is written as

$$s^2 - \{(1 - r_c) + q(r_1 - r_c)\}s + (1 + 2q)(r_2 - r_c r_3) + 4qr_f(r_g - r_4) + \frac{4qr_f(r_2 - r_3 r_g)}{s} = 0 \ . \qquad (6.3a)$$

Equation (6.3a) reduces to the dispersion relation used in the two-dimensional model when the terms corresponding to the third dimension, terms with S_2 [see Eq. (4.12c)], are taken to be zero, and Eq. (4.37a) is used in favor of Eq. (4.36a). As discussed in Section 6, two roots of Eq. (6.3a) can be found which correspond to the two-dimensional mode 1 and mode 2 roots. Thus, when S_2 is relatively small compared to the rest of the terms, the roots of Eq. (6.3a) are identical to those of the two-dimensional model. For a small gap height (< 0.20 mm) or x (< 500 mm), the curves produced by the two models are identical (see Figures 8.5 and 8.6). When the gap height is increased the difference between the two models is still found to be very small.

These results indicate that the velocity in the y-direction dominates the flow field. Furthermore, the two-dimensional model is

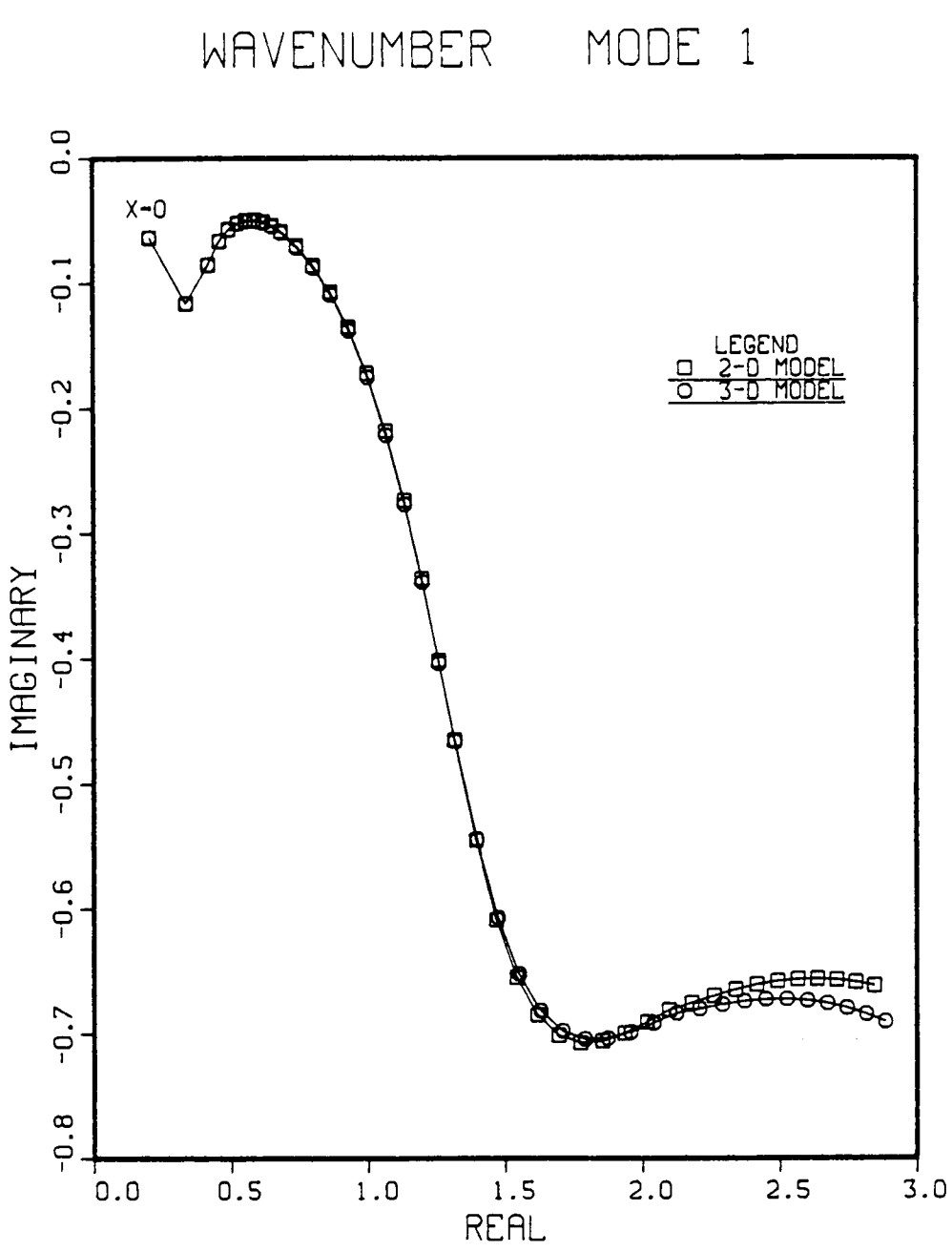


Figure 8.5. Imaginary vs. Real, Complex Wavenumber, Mode 1, 70 Hz., Two-Dimensional and Three-Dimensional Models. Distance From the Stapes Varies From Zero to 1000 mm at 25 mm Increments. Wavenumber is Slightly Different Only at Large Distances From the Stapes.

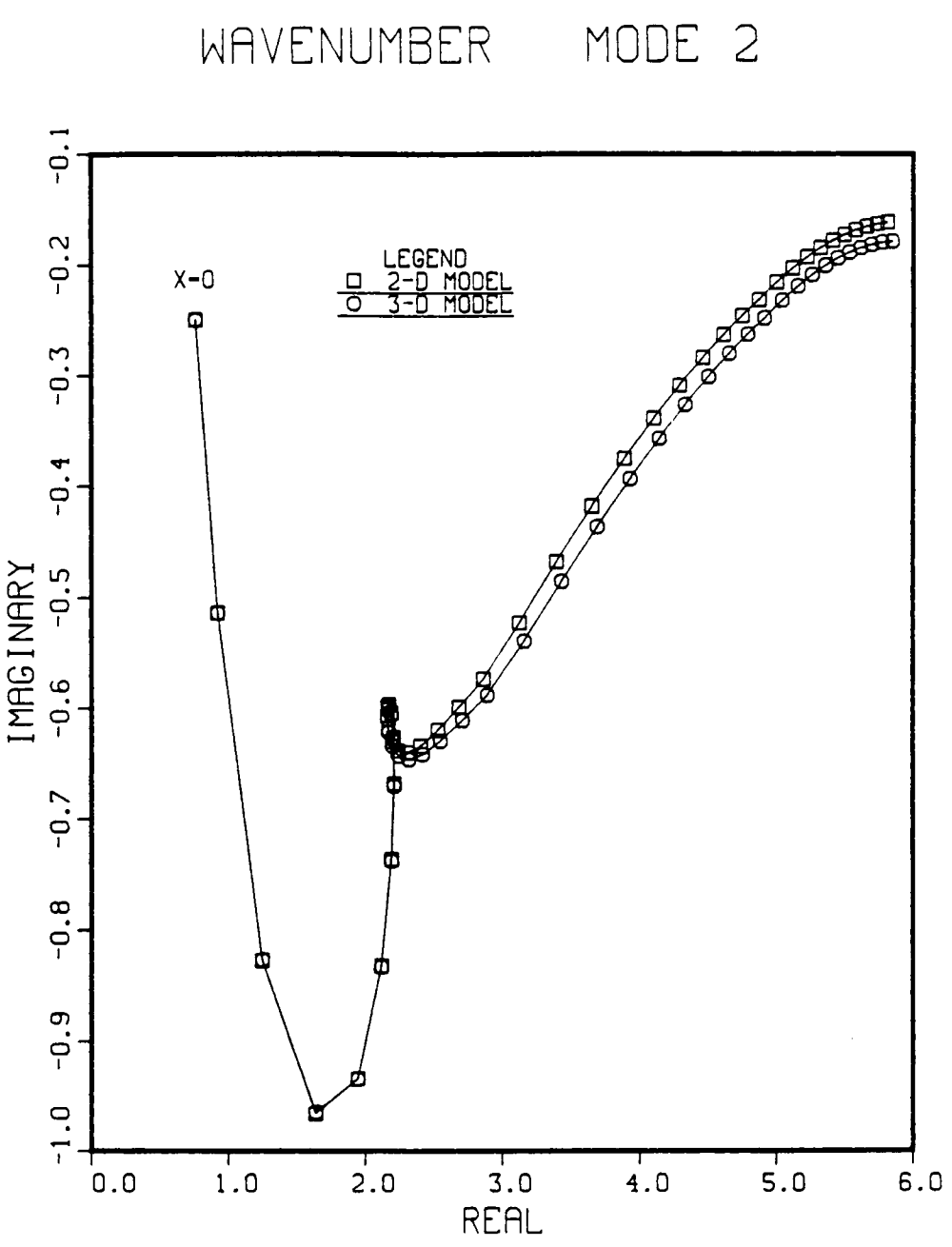


Figure 8.6. Imaginary vs. Real, Complex Wavenumber, Mode 2, 70 Hz., Two-Dimensional and Three-Dimensional Models. Distance From the Stapes Varies From Zero to 1000 mm at 25 mm Increments. Wavenumber is Slightly Different at Larger Distances From the Stapes.

sufficient for determining wavenumbers at $x < 500$ mm. The x and z velocities appear to have very little influence on the wavenumbers. Addition of these fields to the analysis produces a small difference in the wavenumbers. In the overall view, the y velocity predominates the analysis due to the relatively small size of the gap height compared to the width. The three-dimensional model may be more significant when pressures, displacements or velocities are computed. The local effect of the x and z velocities may require further analysis to fully explain their behavior.

9. CONCLUSIONS

Three-dimensional analysis of the gap flow induced by displacement of the blocks yields results that differ qualitatively, but not quantitatively, from those of a two-dimensional analysis. For the three-dimensional model, but not for the two-dimensional model, the resistance offered by the gap fluid to displacement of the blocks depends on the local wavenumber. Also, the three-dimensional flow depends on both relative and absolute block displacements, while the two-dimensional flow depends on only relative displacements. Despite these qualitative differences, the complex quantities (gap flow spring stiffnesses) that express the fluid resistance are numerically almost the same for both the two- and three-dimensional models.

Three-dimensional analysis of the net flow through the gap raises the order of the dimensionless dispersion relation. This suggests that there are three, rather than two, roots (wavenumbers) of the dispersion relation that correspond to modes of propagation. Since the three duct pressures are state variables, three modes of some kind exist even in the two-dimensional model. But there, the third mode is the "static" mode in which all three pressures are equal and no partition displacements occur. The wavenumber of the static mode is zero. In the three-dimensional model, the altered form of the dispersion relation may yield a nonzero wavenumber for

the static mode. If so, the mode would include a propagating wave in the gap in the absence of any partition displacements.

Three-dimensional flow patterns associated with both the net flow and the flow induced by block displacements have not been obtained before. But until the computational model used herein agrees with experimental results, the significance of these flows is indeterminate. Assuming that agreement with experimental results is eventually obtained, we may find the flows derived above to be useful in understanding the operation of the mammalian cochlea. The hair cells, which are the primary transducers in the cochlea, reside in the region corresponding to the gap analyzed above. Furthermore, the mechanism by which the hair cells are stimulated is not known. If stimulation is provided by fluid flow in the immediate vicinity of the hair cells, the analysis presented above may be important.

LIST OF REFERENCES

LIST OF REFERENCES

Boulet, J. A. M. (1984). "The Role of the Inner Sulcus in Cochlear Mechanics," Ph.D. Dissertation, Stanford University.

Conte, S. D. and De Boor, C. (1972). Elementary Numerical Analysis, McGraw-Hill, New York.

Davis, H. (1953). "Acoustic Trauma in the Guinea Pig," J. Acoust. Soc. Am. 25, 1180-1189.

Helle, R. (1974). "Beobachtungen an hydromechanischen Modellen des Innenohres mit Nachbildung von Basilarmembran, Corti-Organ, und Deckmembran," Dr.-Ing. Dissertation, Technische Universitat, Munchen.

Steele, C. R. (1974). "Behavior of the Basilar Membrane with Pure-Tone Excitation," J. Acoust. Soc. Am. 55, 148-162.

Steele, C. R. (1976). "Application of the WKB Method in Solid Mechanics," in Mechanics Today, Vol. 3, S. Nemat-Nasser, ed., Pergamon Press, New York, 243-295.

Whitham, G. B. (1974). Linear and Nonlinear Waves, John Wiley, New York.

VITA

James Barney Holt was born on January 16, 1962, in Jamestown, Tennessee. He attended elementary school in that city and was graduated from Alvin C. York Agricultural Institute in June 1980, where he was valedictorian. He received the Tennessee Farmers Co-op Scholarship and The University of Tennessee Alumni Valedictorian Scholarship. The following September he entered The University of Tennessee, Knoxville, and received the Alumni Upperclass Scholarship in the spring of 1981. In December 1984 he received a Bachelor of Science degree in Engineering Science, graduating with High Honors.

In January 1985 he was admitted to a Master's program at The University of Tennessee, Knoxville. He received his Master of Science in Engineering Science in June 1986.

In May 1986 James married Kimberly Ann Jones.

James is a member of Golden Key National Honor Society and Tau Beta Pi, Alpha Epsilon Delta, and Phi Eta Sigma honor societies.